Transit Observations of Exoplanets TrES-5-b, HAT-P-23-b, and Kepler-412-b

Alex Koenig

12.410 Project Report

1.   Abstract

The transit depths and planetary radii of exoplanets TrES-5-b, HAT-P-23-b, and Kepler-412-b were studied in order to increase measurement accuracies of previous studies in the literature. One partial transit of TrES-5-b, one full transit of HAT-P-23-b, and one partial transit of Kepler-412-b were observed at the Wallace Astrophysical Observatory. The TrES-5-b transit was statistically significant at the 29% level, and was found to have a transit depth of 2.16±0.84%, corresponding to a planetary radius of 1.22±0.24 R_{Jup}. The HAT-P-23-b transit was statistically significant at the 26% level, and was found to have a transit depth of 1.53±0.32%, corresponding to a planetary radius of 1.44±0.17 R_{Jup}. The Kepler-412-b transit was statistically significant at the 49% level, and the exoplanet was found to have a transit depth of 0.13±0.31%, corresponding to a planetary radius of 0.45±0.54 R_{Jup}. However, it is likely that only the transit brightness of Kepler-412-b was measured, and the observations missed the transit egress. Additionally, the transit duration of HAT-P-23-b was determined to be 2.0±0.22 hours. Except for the Kepler-412-b transit, these results agree with the findings of Maciejewski (2016) and Bakos (2011) regarding TrES-5-b and HAT-P-23-b respectively.

2. Project background
2.1. Exoplanet observations background

Finding exoplanets is of key interest to understanding our solar system in the context of other solar systems, and in determining whether planets like Earth are common or rare. The sample size of known exoplanets has dramatically increased since the first exoplanet discovery in 1992 (Wolszczan 1992); to date, there are approximately 4,000 known exoplanets (Schneider 2019). All of these discoveries have advanced the community's knowledge about the context of our own planet in relation to others, and whether there are more planets like it. Understanding the various types of planets that exist also contributes to our understanding of how star systems form and what kinds of planets the formation process usually creates.

In this project, the light curves for transits of exoplanets TrES-5-b, HAT-P-23-b, and Kepler-412-b will be obtained. An exoplanet transit is when an exoplanet passes between us and its host star, slightly dimming the light of the host star for the duration of the transit. The light curve generated from such an event is shown in Figure 1 below. Such a light curve allows for the determination of the planet's radius via the depth of the curve and the planet's orbital period via the time between transits.
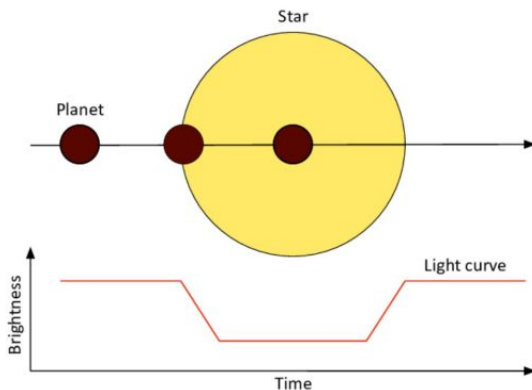

Fig.1: Exoplanet transit. As the exoplanet crosses in front of its host star, which happens once per orbit, some of the star's light is blocked. (Cowley 2014)

The three exoplanets studied in this project are classified as hot Jupiters, which are gaseous planets orbiting close to their host star. Since such planets do not exist within the Solar System, we can only study them through observing other star systems. The mechanism of the formation of hot Jupiters is disputed. One theory is that such planets form in situ close to their host star; another theory is that they form similarly to Jupiter, and then migrate closer in to their host star (Dawson 2018). This project aims to narrowing the uncertainty of the size and transit duration of three such hot Jupiters in order to contribute to our knowledge of their formation. Although these parameters are well-known for the exoplanets for this project, any further data can help to refine those parameters for general study within the astronomical community.

2.2. Project goal
2.2.1. Selection of target exoplanets

In order for the telescope equipment to be technically capable of detecting a transit, observational requirements are as follows: the exoplanet must be above the horizon during the night, with an altitude of greater than 30 degrees; the visual magnitude of the host star must be between 6 and 14; and the change in magnitude of the star during the transit must be greater than 0.01. Furthermore, the transit must either begin after 21:00 or end before 00:00 on the

night of observation to detect a partial transit, and it must both begin after 21:00 and end before 00:00 to detect a full transit. This requirement is because the available observing window on each night is 20:30 to 00:30, and 30 minutes of observation are required either before or after the transit for two purposes: (1) in order to compare the transit brightness of the host star to its baseline brightness, and (2) to determine when the transit begins and/or ends.

These strict observational criteria narrowed down the exoplanet selection process to include TrES-5-b, HAT-P-23-b, and Kepler-412-b. The selection process used the Exoplanet Transit Finder (Jensen 2013).

2.2.2. Target Exoplanets: Hot Jupiters TrES-5-b, HAT-P-23-b, Kepler-412-b

The following table contains the position, magnitude, and transit duration of the exoplanets used in this project. These parameters were the most important in choosing the target exoplanets. Their position ensures they would be above the horizon during the night of the observation; their magnitude and transit depth ensures the telescopes would have a great enough signal-to-noise ratio to detect the transit; and their transit duration ensures the transits would take place within a single observation session. In the table, coordinates, magnitudes, transit depths, and transit duration are provided by Jensen (2013).

Table 1: Target exoplanets observed in the project.

Exoplanet	RA, Dec (J2000)	Mag (apparent)	Transit depth (%)	Transit duration
TrES-5-b	20:20:53, +59:26:56	13.72	2.04	1 hr 48 min
HAT-P-23-b	20:24:30, +16:45:44	12.43	1.40	2 hr 10 min
Kepler-412-b	19:04:26, +43:40:51	13.73	1.04	2 hr 11 min

TrES-5 is one of the faintest transiting planet host stars discovered from the ground (Maciejewski, 2016); therefore, TrES-5-b will present an interesting technical challenge for this project, given that its faint transit will push the limits of the observing equipment. The planet's radius was determined to be 1.209±0.021 R_{Jup} (Maciejewski, 2016). A 2015 follow-up study of TrES-5-b confirmed this radius (Mislis, 2015).

HAT-P-23b was first discovered using the transit method at the Keck Observatory in 2011, with a period of 1.212884±0.000002 days and a size of 1.368±0.090 R Jupiter (Bakos et al., 2011). Further transit detections using three small telescopes with the telescope-defocussing technique in 2015 gave a smaller size of 1.224±0.037 $R_{Jupiter}$, although this new work agreed with the previous orbital period determination (Ciceri et al., 2015). Each of these size determinations is outside of the uncertainty range for either, suggesting a possible as-of-yet unresolved disagreement between the two.

Kepler-412b was first discovered using the transit method by the Kepler space telescope in 2014, with a size of 1.33±0.04 $R_{Jupiter}$ (Deleuil et al., 2014). This planetary radius was confirmed by Angerhausen et al. in 2015.

3. Data

3.1. Equipment at the Wallace Astrophysical Observatory

Equipment at the Wallace Astrophysical Observatory provided the data taken in support of this project. Specifically, data were acquired with a Celestron C14 telescope with a SBIG STL-1001e CCD and open filter. Observations of TrES-5-b and HAT-P-23-b used pier 2; observations of Kepler-412-b used pier 4. The open filter provided highest photon throughput of all available filters in order to achieve the signal-to-noise ratio required for this project.

3.2. Data collected in support of the project

Over the duration of the available observation sessions, a total of three nights of data were captured on three separate partial exoplanet transits. Adverse conditions affected data acquisition on each night: on the first night, partial clouds blocked sections of the sky, forcing the selection of an alternate exoplanet transit; on the second night, the sky became hazy just as the transit was predicted to end; on the third night, although the sky was clear, the full moon degraded data quality due to increased background signal.

Generally, the required signal-to-noise ratio to observe the exoplanet transit determined the exposure times for each night via the following equation, which assumes a photon-noise-limited signal-to-noise ratio:

$$SNR^2 = QE * A_{Telescope\ Aperture} * bandwidth * \Delta t * F_0 * 10^{-0.4*magnitude} \qquad (1)$$

The required signal-to-noise ratio on the measurement of overall star brightness is one that is large enough to differentiate the baseline star brightness and the transit brightness. For example, with a transit depth of 2%, the required signal-to-noise ratio is $\frac{1}{2\%} = 50$ at a minimum. A signal-to-noise ratio several factors greater than this minimum value is preferred in order to determine the depth of the transit with greater precision, and to have a sufficient margin in case factors unaccounted for in the above equation also affect the noise.

For example, the third night of observation was during a full moon, and so the chosen exposure time was longer than the above equations suggests is necessary. On that night, so as to maximize the possibility of observing the transit, the exposure time was instead chosen such that the star would be in the upper end of the linear CCD regime, at approximately 50,000 photon counts per pixel. Due to the variability of the point spread function of stars on any given night, the exposure length necessary to achieve this specification was determined experimentally on the night of observation rather than analytically beforehand.

For the other nights, the exposure time from the above equation was arbitrarily multiplied by a factor of 10. The predicted SNR is therefore a factor of 3 greater than the minimum required to observe the transit.

The table below summarizes the data collected in support of this project. Predicted transit times are provided by Jensen (2013) in *Tapir: A Web Interface for Transit/Eclipse Observability*. Note for each night the discrepancy between the observation times and the predicted transit times. These discrepancies, caused by restrictions in available observation times at the Wallace

Astrophysical Observatory, result in the observation of only partial rather than full transits of all but potentially the second night of observations.

Table 2: Summary of Collected Data

Date (UTC)	Target exoplanet	Equipment: Pier Filter Binning	Frames acquired	Exposure time (sec)	Observation start / end (UTC) & duration	Predicted transit start / end (UTC) & duration	Conditions
2019-09-25	TrES 5 b	Pier 2 Open filter 1x1 binning	Light (42)	100	03:04 / 04:21 (1 hr 17 min)	02:12 / 04:00 (1 hr 48 min)	Partially cloudy
			Bias (20)	0			
			Dark (4)	100			
2019-10-06	HAT P 23 b	Pier 2 Open filter 1x1 binning	Light (74)[1]	120	01:20 / 03:59 (2 hr 39 min)	01:19 / 03:29 (2 hr 10 min)	Increasingly hazy at end of night
			Bias (20)	0			
			Dark (4)	120			
2019-10-16	Kepler 412 b	Pier 4 Open filter 1x1 binning	Light (15)	400	01:22 / 03:04 (1 hr 42 min)	00:30 / 02:41 (2 hr 11 min)	Sky clear Full moon
			Bias (21)	0			
			Dark (3)	400			

[1]Frame 19, taken at approximately 02:00, corresponds to the frame in which the telescope was temporarily moved to further retract the roof of the observatory. The data from this frame are unusable.

In addition to these frames, 12.410 staff collected flat frames corresponding to the appropriate telescope, open filter, and 1x1 binning of the above data. Flat frames are discussed further in Section 4.1.

4. Data processing
4.1. Image calibration
4.1.1. Necessity of calibration techniques

CCD images such as those taken for this project come with a variety of sources of systematic CCD error which can be to some extent calibrated for in the data. In this project, calibration techniques account for three particular types of signal: read signal, dark signal, and flat error. Read signal is the signal produced as a byproduct of the CCD transferring electrons captured in each pixel to the analog-to-digital signal converter. Since the CCD cannot measure negative voltages, which may otherwise exist if the read noise is too large, the voltages of each pixel are artificially raised in order to keep a positive voltage on all pixels. Dark signal, also known as thermal signal, is the signal resulting from charge generated by the thermal motion of atoms in the CCD. Flat variation is the variations produced both by the optical system through vignetting and dust spots, and by the CCD through differences in the quantum efficiency of each pixel.

The use of calibration techniques account for the estimated average offsets in individual pixel brightnesses due to the factors described above. Bias frames measure the average read signal for each pixel, which then can be subtracted from each corresponding pixel in the light frames so as to only leave the true signal and other extant sources of noise and error. Dark frames measure the average dark signal for each pixel, which are also subtracted in the same manner. Flat frames measure photon throughput of individual pixels. Since flat frames correspond to relative photon throughput of each pixel, data are divided by the flat frame measurements. For example, if one pixel collected half as much light as another when it should have collected the same amount, the division of the flat frame multiplies the signal from the weaker pixel by a factor of two.

4.1.2. Acquisition of image calibration frames

Calibration frames were acquired in the following manner:
Before or after each observation session, a total of approximately 20 bias frames were collected by using a closed filter on the CCD with a 0-second exposure time so as to only capture bias signal. These data were taken before the observation session on the first night to make use of observation time during a full cloud cover, and were taken after the observation sessions on the second and third nights so as to not miss any transit data by instead collecting image processing frames during the transit.

After each observation session, 3-4 bias frames were collected by using a closed filter on the CCD with an exposure time corresponding to that of the light frames, in order to match the dark signal of the light frames.

Observatory staff collected flat frames corresponding to the appropriate 1x1 pixel binning and open filter used for this project. Flat frames were acquired by directing the telescope at an evenly lit patch of the sky and taking exposures at an appropriate length to bring each pixel into the linear photon regime.

4.1.3. Calibrating images

Having multiple bias, dark, and flat frames enables the calculation of an average error across each set, since the error for each pixel varies from frame to frame, whereas the average error for each pixel is constant. Also relevant is that while bias frames only contain bias signal, dark frames actually contain both bias signal and dark signal, and flat frames contain read signal,

dark signal, and flat variation. The following equations describe how the sets of bias, dark, and flat frames provide average read signal, dark signal, and flat correction values for each pixel:

$$Master\ bias\ =\ avg(bias\ value\ in\ each\ bias\ frame) \tag{2}$$

$$Master\ dark\ =\ avg(dark\ value\ in\ each\ dark\ frame)\ -\ master\ bias \tag{3}$$

$$Master\ flat\ =\ \frac{avg(flat\ frame\ value)\ -\ master\ dark\ -\ master\ flat}{avg(pixel\ value\ in\ the\ central\ 100x100\ pixels\ of\ the\ flat\ frames)} \tag{4}$$

These read signal, dark signal, and flat correction factors are each part of a master bias frame, master dark frame, and master flat frame respectively. Note that the observatory staff produced the master flat frames for this project with their own bias frames and dark frames. Their dark frames corresponded to the exposure time of the collected flats rather than the lights.

As described in Section 4.1.1., subtracting the bias and darks from the light frames and then dividing by the flats provides a more accurate set of corrected light frames:

$$Corrected\ light\ frame\ =\ \frac{raw\ light\ frame\ -\ master\ dark\ -\ master\ bias}{master\ flat}. \tag{5}$$

Specifically, this equation describes the process to correct each pixel in each light frame, and uses the corresponding pixels from the master bias, dark, and flat frames. The python code performing image processing as described above is located in Appendix 8.1.

To verify image processing, compare a raw inverted light frame with a corrected light frame from the third observation night, as shown in the figure below. Kepler-412, the exoplanet host star, is circled in red in each frame. Although the corrected light frame is still not perfect in terms of being evenly lit across the frame, the data were certainly improved upon application of the image processing frames, and so the reduction success is acceptable. Specifically, in the raw frame, there is an approximately 20% gradient between the brightest and dimmest portions of the frame; this gradient decreases to approximately 10% in the processed frame.
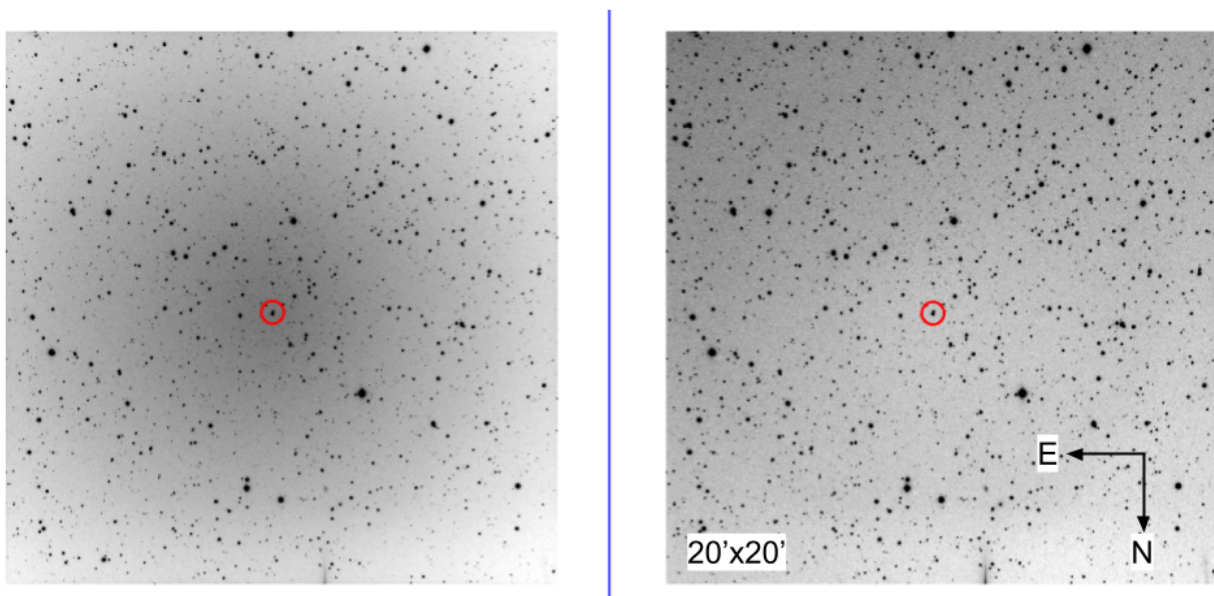

Fig.2: Example light frame, pre-processing (left) and post-processing (right). The light gradient across the frame was reduced by a factor of two.

4.2. Plate solving
4.2.1. Necessity of plate solving techniques

It is not feasible to use the pixel coordinates of the exoplanet host star on each frame in order to perform photometry, since the pixel coordinates of the star change slightly over the course of the night; instead, we use the true sky coordinates of the star, which are provided by plate solving techniques which enable us to map true sky coordinates to pixel coordinates. The pixel coordinates of the star change during each observation session because although the telescope is pointed approximately at the exoplanet host star for the duration of the observation session, the star moves a slight amount between each frame due to tracking errors in the telescope mount. Referencing the same pixel coordinates between two frames will miss the star signal when the star shifts over to neighboring pixels in the next frame.

The figure below depicts the movement of exoplanet host star Kepler-412 in the frame over the course of the night, showing the first light exposure on the left and the last light exposure on the right. Each frame is cropped to approximately 2'x2'. The red circle remains at the same pixel coordinates, while the Kepler-412 shifted down by 10 pixels and to the right by 9 pixels. Since the star moved pixel coordinates, photometric measurements by reference to pixel coordinates are ineffective.
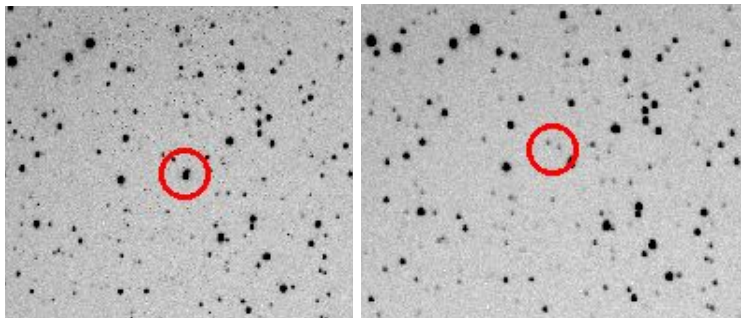

Fig.3: Inverted light frames depicting the movement of Kepler-412 between frames. The star shifted pixel coordinates while remaining at the same right ascension and declination, rendering photometric measurements by reference to pixel coordinates ineffective.

4.2.2. Plate solving software

Software provided by astrometry.net determines the true right ascension and declination coordinates of each pixel in each light frame (Lang 2010). Their software creates a list of all the pixel locations of stars in the frame, and compares that arrangement of stars to star index files in the sky surrounding the approximate telescope position. Once it finds a match and determines the sky coordinates of the center of the image from that match, it maps each pixel coordinate in the frame to a true sky coordinate, which it provides through a new .fits file containing both the original light frame and the coordinate mapping. This coordinate mapping is not perfectly linear due to field curvature of the focal plane not aligning with the flat CCD sensor.

The python code interfacing with the astrometry.net plate solving software to implement the above methods is located in Appendix 8.2. The code header contains instructions to install and run the plate solving software. In the python code, it is necessary to specify the approximate field location of each image, the images to perform the plate solving on, and the size of the search radius around the approximate field location to find star index matches.

4.3. Photometry
4.3.1. Photometry overview

Photometry techniques enable the determination the signal of the host star over the duration of the observation session. These data provide the light curve of the exoplanet transit, which contains the information necessary to determine exoplanet parameters.

Photometry, in its most basic form, is the summation of pixel signal counts for the pixels that contain the exoplanet host star signal. However, this summed pixel count includes both the exoplanet host star signal and the background sky signal. The difference between the summed pixel count and the background sky count gives the true signal for the host star. The average value of pixels nearby the star that do not contain the star signal provide a measure of the background sky count for this subtraction.

4.3.2. Apertures

In each light frame, one virtual circular aperture is centered on the star, and one virtual annulus aperture surrounds the circular star aperture, also centered on the star. The sum of the signal in the pixels of circular aperture is the sum of background signal and star signal. The sum of the signal in the annulus aperture is only the background signal, since the latter aperture does not contain the star pixels. Since the amount of background signal in each aperture depends on how many pixels are in each, in order to subtract the correct amount of background noise from the circular aperture signal, the relative areas of the apertures $A_{circular}/A_{annulus}$ multiplies the annulus aperture signal before the subtraction.

The optimal aperture size is the one that achieves the best signal-to-noise ratio in the resulting photometric data. The optimal aperture size depends on the point spread function of the stars on a given night of observation, so the optimal size will change from night to night, and thus must be calculated for all nights separately.

The standard deviation of the mean of a group of points in the data provides a measure for the signal-to-noise ratio, and so this standard deviation can be compared across aperture sizes to select the best aperture size, which corresponds to the lowest found standard deviation. Note that the photometric data used in this calculation are those from the relative host star brightness calculations using various on-frame reference stars, as explained in 4.3.3., "Reference stars." Also note that for simplicity, all stars for a given night of data had the same virtual aperture sizes, both host star and reference stars included.

Comparing the standard deviation of the same group of points while varying the size of the circular aperture provides the following figure, which demonstrates that for the 2019-09-25 night of observation, the best circular aperture has a radius of 7.75 pixels. In the plot, all standard deviations are measured relative to the standard deviation of data at the optimal aperture size.
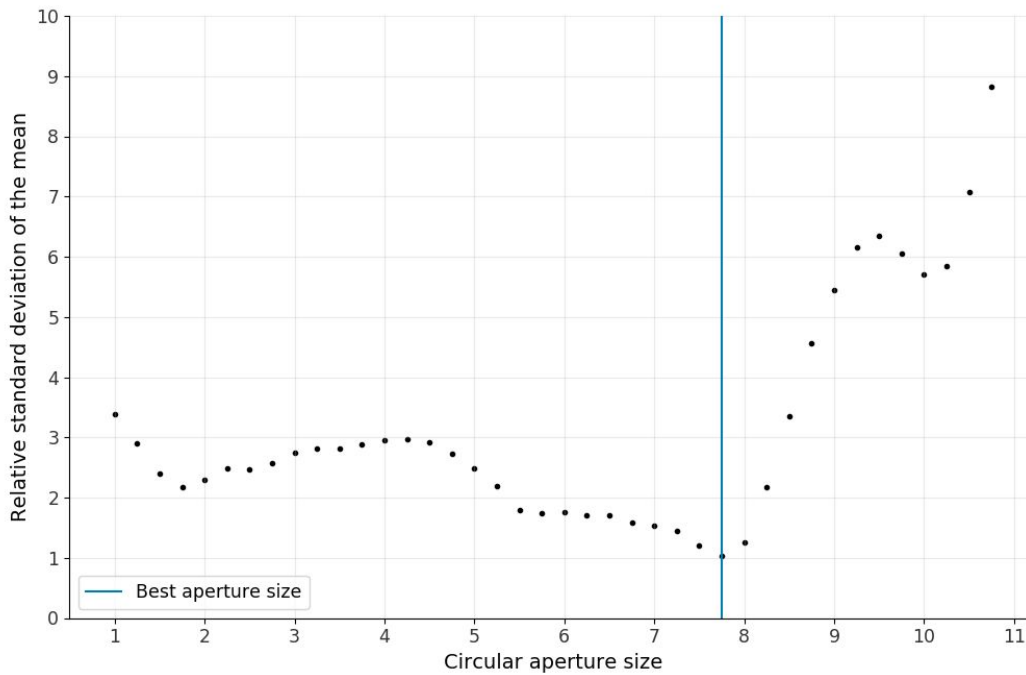
Fig.4: Relative standard deviation of photometric data from the 2019-09-26 night of data with a variety of virtual circular aperture radii. The best circular aperture size is shown to have a radius of 7.75 pixels.

In this plot, however, the sky aperture is arbitrarily chosen to have inner and outer radii which are respectively two and four pixels larger than the circular aperture. Other plots with different inner and outer radii differences verify whether other sky aperture sizes will improve the signal-to-noise ratio of the data. The first figure below uses sky aperture radii of three and five pixels larger, respectively; the second figure below uses sky aperture radii of one and four pixels larger, respectively. All standard deviations are measured with respect to the best standard deviation from the previous figure with a circular aperture size of 7.75 pixels.

Each plot below demonstrates a higher standard deviation and thus worse signal-to-noise ratio compared to the first plot above, suggesting that the best aperture radii for this night of data are 7.75 pixels for the circular aperture, 9.75 pixels for the inner radius of the sky aperture, and 11.75 pixels for the outer radius of the sky aperture. Note that the optimal circular aperture sizes change when the chosen sky aperture sizes change. Physically, it is not intuitive that this effect should exist, since the best circular aperture size should not depend on how the background signal is measured, only on the point spread function of the star.

One possible explanation for this effect is that other faint stars exist nearby the exoplanet host star in the frame, and different sky aperture sizes include their signal in the background counts in different amounts depending on their radii. Since sky aperture sizes are dependent on the circular aperture size as a result of having radii specified to be a certain number of pixels larger, the best circular aperture size changes from that specification.

The plot below displays relative standard deviation of photometric data from the 2019-09-26 night of data with a variety of virtual circular aperture radii, and chosen inner and outer sky

aperture radii of circular radius + three pixels and circular radius + five pixels respectively. The lowest achievable standard deviation is approximately 50% more than that of the plot above, which used sky aperture radii that were each one pixel smaller.
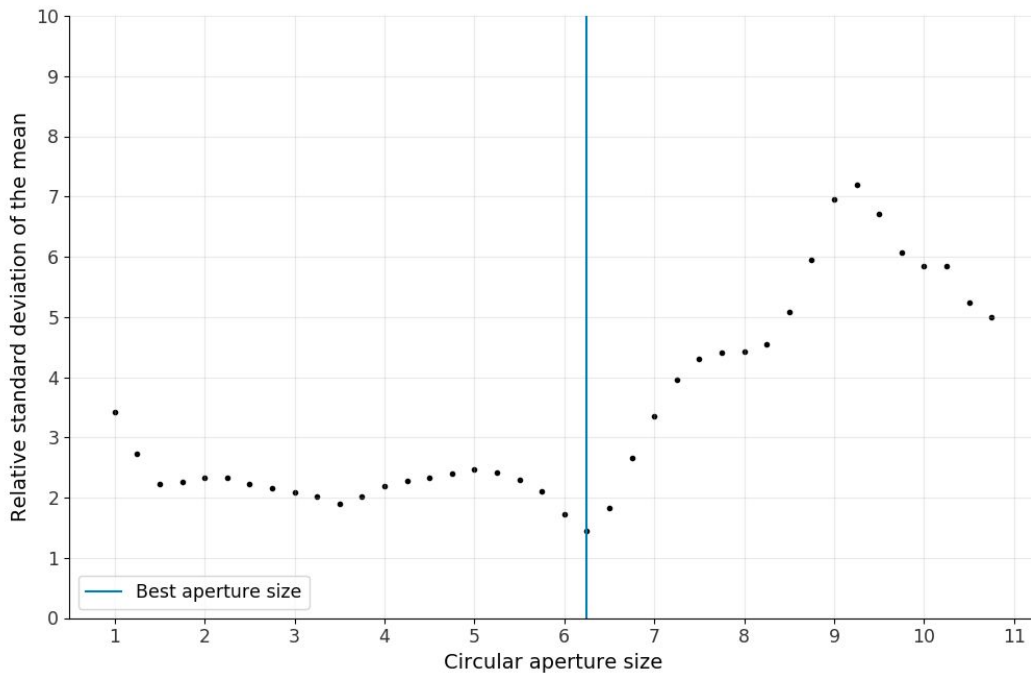

Fig.5: Relative standard deviation of photometric data from the 2019-09-26 night of data with a variety of virtual circular aperture radii, with increased sky aperture radii. The lowest standard deviation increased by 50% from the previous plot.

The next plot displays relative standard deviation of photometric data from the 2019-09-26 night of data with a variety of virtual circular aperture sizes (radii), and chosen inner and outer sky aperture radii of circular radius + one pixel and circular radius + three pixels respectively. The lowest achievable standard deviation is approximately 100% more than that of the first plot, which used sky aperture radii that were each one pixel larger.
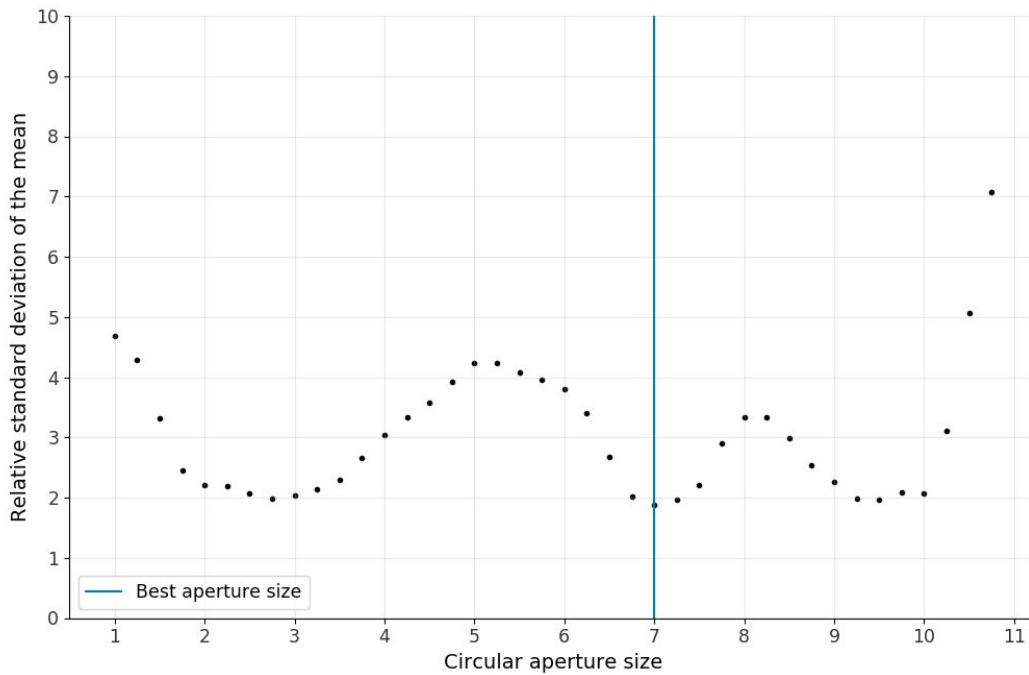
Fig.6: Relative standard deviation of photometric data from the 2019-09-26 night of data with a variety of virtual circular aperture radii, with decreased sky aperture radii. The lowest standard deviation increased by 100% from the first plot.

Repeating this procedure for all three nights of data provided optimal aperture sizes for each night, which are provided in the table below. In the table, note that optimal sky aperture radii for the second observation night are approximately twice the size of those for the first and third night of observations. One possible explanation is that these large sky aperture radii avoid selecting signal from stars close to the exoplanet host star on the frame. Inspection of a light frame from the second night of data reveals several stars within approximately 20 pixels of Kepler-412, and a sky aperture of empty space surrounding that region, providing support for this explanation. See Appendix 8.4. for the frame.

Table 3: Optimal aperture sizes for each night of data

Date (UTC)	Optimal circular aperture radius	Optimal sky aperture inner radius	Optimal sky aperture outer radius
2019-09-26	7.75	9.75	11.75
2019-10-06	5.75	19.5	20
2019-10-16	5.25	6.25	8.25

4.3.3. Reference stars

Even with the background sky noise subtracted from the star signal counts, the signal from the exoplanet host star changes over the course of the observation session due to changing atmospheric seeing conditions and a changing amount of airmass that star signal passes through before reaching the telescope. Depending on whether the star is rising or setting, the

signal from the star will respectively increase or decrease over the course of the night. The following graph depicts the exoplanet host star signal from the second night of data collection, when the host star was setting in the sky and the sky also got hazy towards the end of the night. The changing atmospheric conditions obscure any information on the true change of brightness of the star over the course of the night. The signal from the star decreases over the course of the night due to the star's decreasing altitude, as seen in exposures 1-50, and due to increasing haziness in the sky, as seen in exposures 50-70.
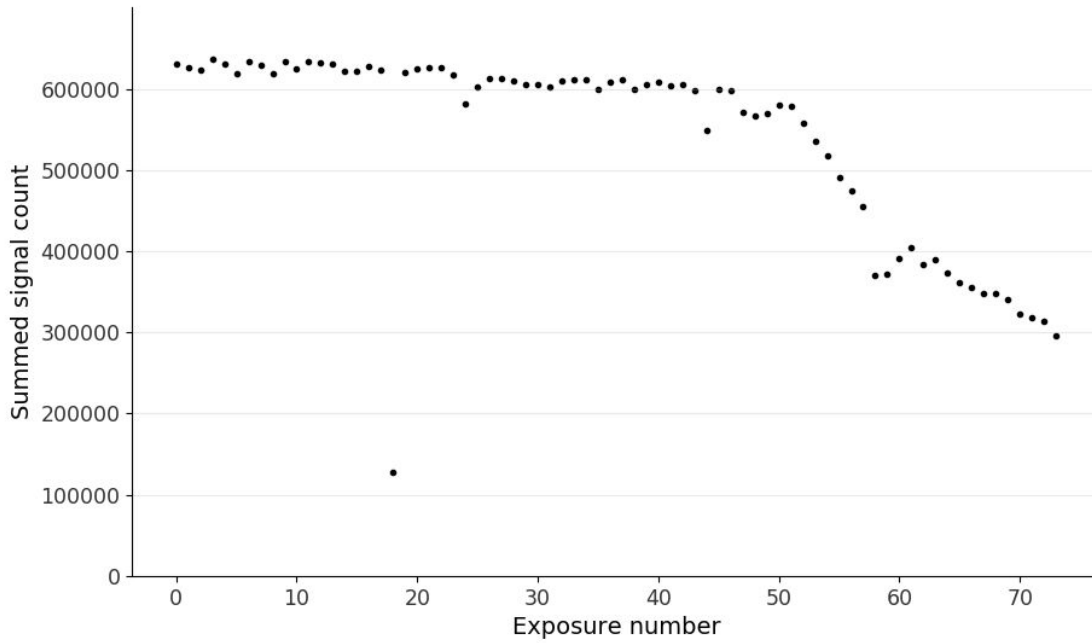

Fig.7: Summed star signal count of HAT-P-23 for each exposure on the 2019-10-16 night of observation. No transit is observable in this unreferenced data.

Atmospheric conditions reduce the brightness of affect all stars on the frame by the same factor, however, and so the relative brightness of the host star and other stars on the frame is constant, except for the variation in host star brightness due to the exoplanet transit. Therefore, dividing the signal of the host star by the average of several reference star signals reveals the true transit light curve. Consider the following figure, which displays another on-frame star's summed star signal count along with that of HAT-P-23.
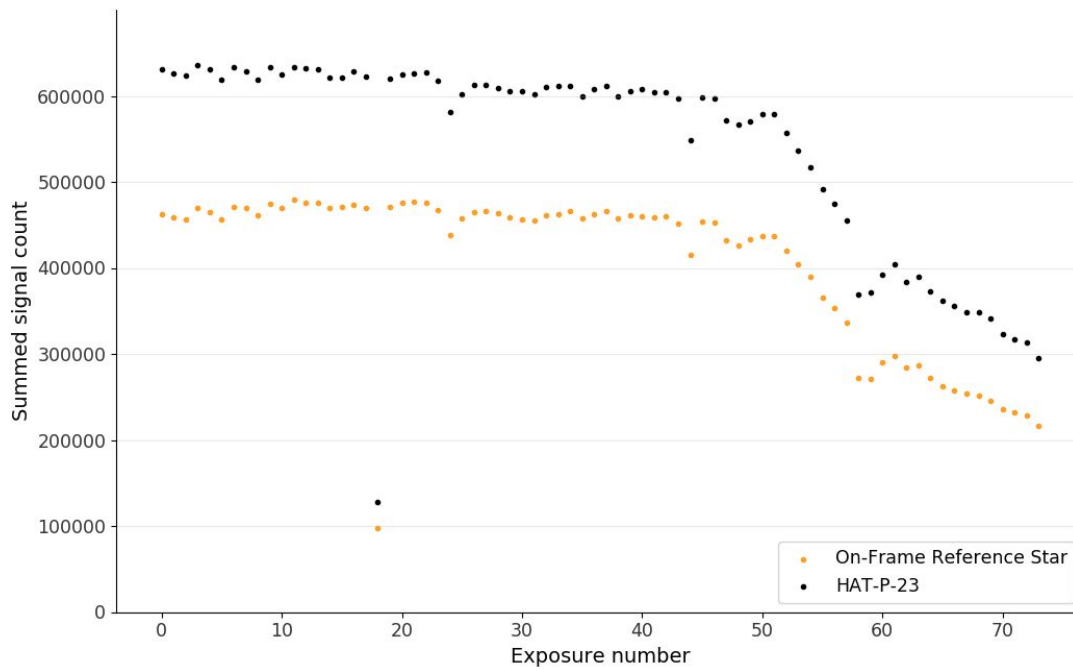
Fig.8: Summed star signal count of HAT-P-23 along with a chosen on-frame reference star. Although the brightnesses of each star varies due to changing atmospheric conditions, the variation in each follows a similar trend over the course of the night.

Reference stars can therefore extract the change in the host star signal due to a transit rather than due to atmospheric conditions. Not all of the other stars on the frame are appropriate for use as reference stars, however. The first criteria for selection of reference stars is that they be located approximately in the same region as the host star on the frame, since the flat correction did not remove all the light gradient in the frame, and so only the signals of the stars closest to the host star will be affected the same by changing atmospheric conditions. The second criteria is that the reference stars themselves cannot have variable brightness. Checking that a given reference star is constant relative to several other reference stars in the frame ensures that reference star meets this criteria. The third criteria is that the signal from the reference star must have an acceptable signal-to-noise ratio. Any noise in the reference star will also contribute noise to the relative host star signal, and thus decrease the signal-to-noise ratio of the resulting transit light curve.

The following figure depicts the brightness of a candidate reference star on the frame relative to the average brightness of three other candidate reference stars. Note that the brightness of the candidate reference star does not remain constant. Therefore, this candidate reference star is inadequate for use in the final creation of the host star light curve. Repeating this process for several candidate stars reveals those that are adequate for use as reference stars.
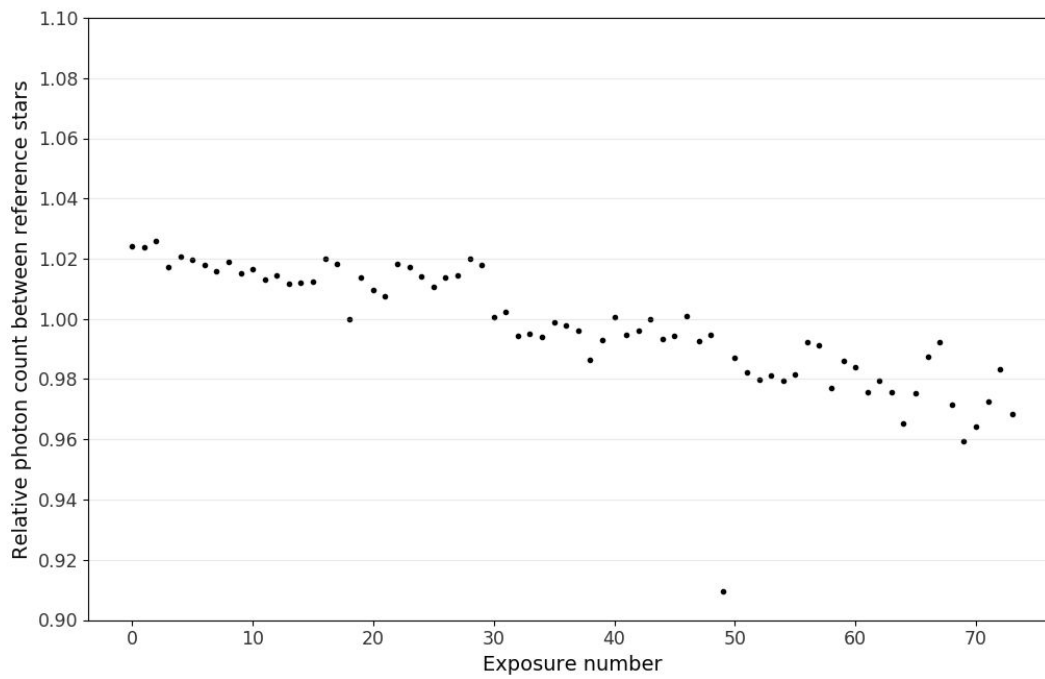
Fig.9: Rejected candidate reference star. The brightness of this candidate star varies with respect to other reference stars, and this candidate star is therefore unsuitable for use as a photometric reference.

The following figure depicts the brightness of a candidate reference star on the frame relative to the average brightness of five other candidate reference stars from the second night of observations. Note that in this figure, the brightness of the candidate reference star remains constant.
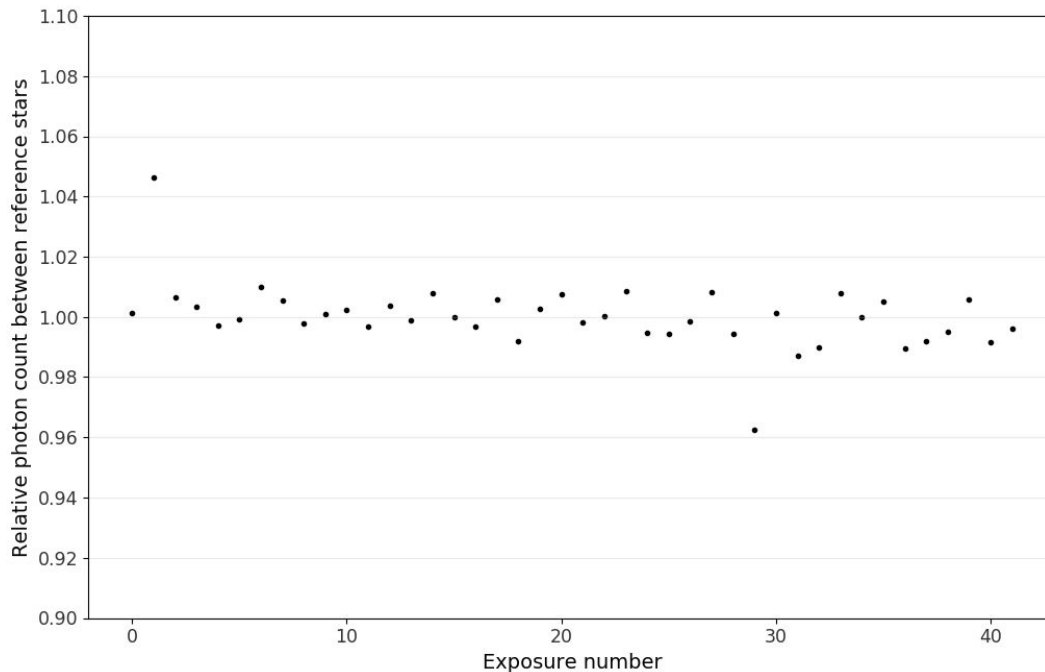
Fig.10: Accepted candidate reference star from the 2019-09-25 night of observation. Although there are two exposures with outliers of ±4% brightness, most of the data fall within ±1% of the mean, and the relative brightness of the star remains roughly constant over the course of the observation session.

The photometric analysis of TrES-5-b incorporated six reference stars, while that of HAT-P-23-b incorporated three reference stars, and that of Kepler-412-b incorporated five reference stars. A roughly equal amount of time was spent searching for and verifying reference stars on each night. The difference in number of reference stars used reflects the relative difficulty in finding acceptable reference stars for each night of data.

4.4. Transit light curves
4.4.1. Initial transit light curves

Applying the data reduction, plate solving, and photometric techniques as described in 4.1., 4.2., and 4.3. respectively provide transit light curves for each night of data, which are shown below. Possible observed transit ingresses and egresses, determined visually, are plotted compared to predicted ingress and egress times from Jensen (2013), along with predicted transit depths from Jensen (2013). For a discussion of the potential causes of such timing errors, see Section 5.5. Note that the data are not binned, and are normalized to the baseline brightness of the host star in each plot. The calculation of the baseline brightness will be explained in Section 4.2.2.

The figure below shows the light curve of TrES-5-b on the night of 2019-09-26. Observations were taken with 42 100-second exposures. The decreased signal-to-noise ratio towards the start and end of the observation session correspond to partial clouds observed during the data collection process. Visually, the transit appears to end potentially at around 03:40, which is 20 minutes before the predicted end of the transit at 04:00.
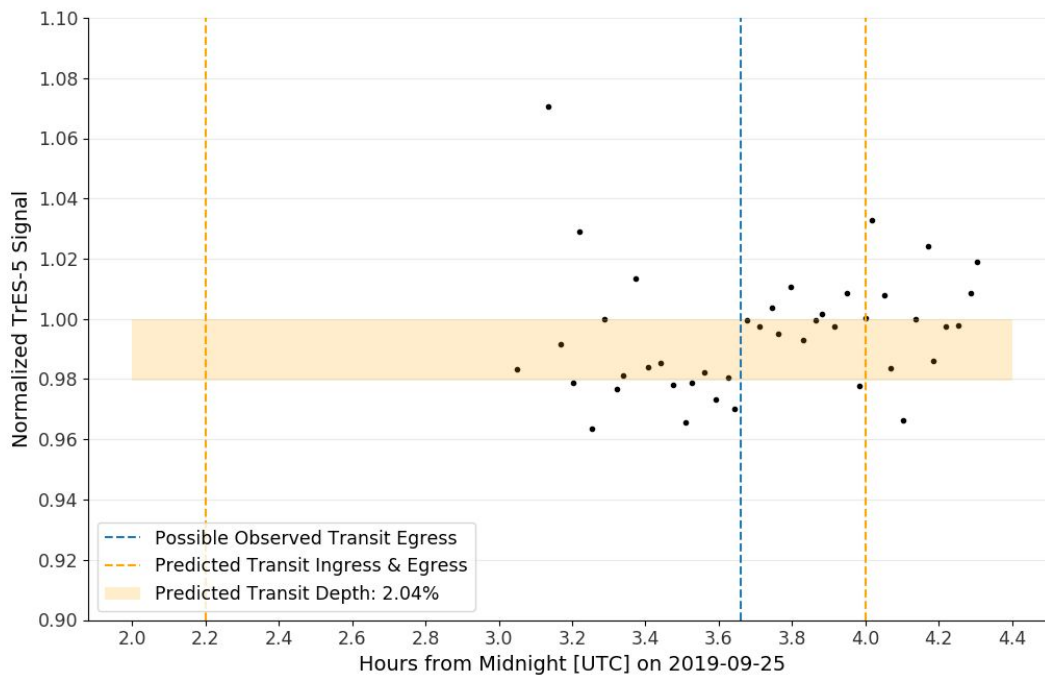
Fig.11: Light curve of exoplanet TrES-5-b. The transit appears to end ~20 minutes early.

The figure below shows the light curve of HAT-P-23-b on the night of 2019-10-06. Observations were taken with 74 120-second exposures. The increased signal-to-noise ratio towards the end of the observation session corresponds to haze observed during the data collection process. Visually, the transit appears to potentially start and end approximately 17 minutes and 9 minutes after the predicted times respectively.
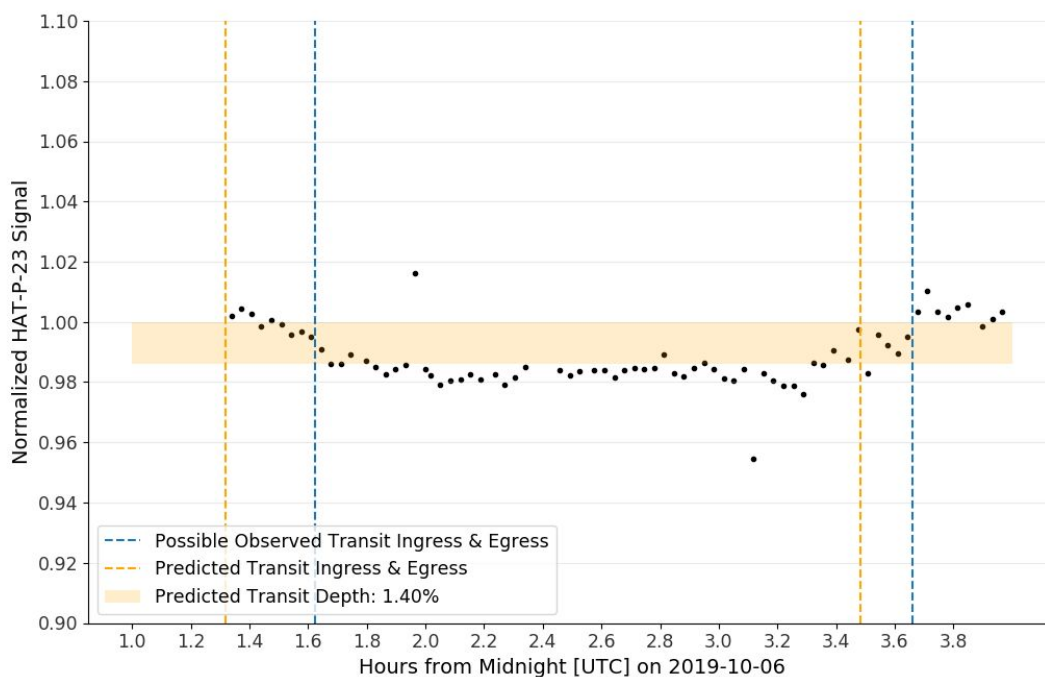

Fig.12: Light curve of exoplanet HAT-P-23-b. A full transit appears to have been observed.

The next figure displays the light curve of Kepler-412-b on the night of 2019-10-16. Observations were taken with 15 400-second exposures. There is no discernible increase of brightness at the predicted end of transit.
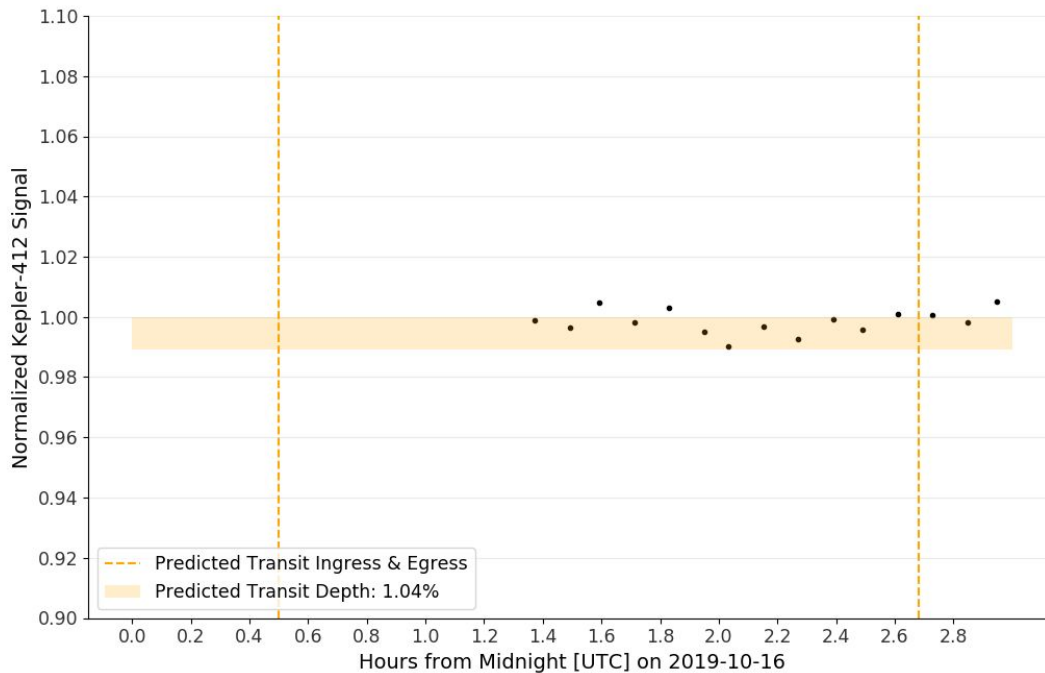

Fig.13: Light curve of exoplanet Kepler-412-b. No transit is visually observable.

4.4.2. SNR calculation for each night of data

The actual achieved signal-to-noise ratio in these transit light curves comes from the following equation:

$$SNR = \frac{\mu}{\sigma}. \tag{6}$$

In later analysis of error estimation of the transit depth, it will prove useful to calculate the signal-to-noise ratio for different times during each night. In general, the noise throughout the night varied due to varying atmospheric conditions. Some sections of the data may prove to have a lower signal-to-noise ratio and thus be more useful for transit depth estimation.

The plots below show the change in signal-to-noise ratio of the signal throughout the night. The signal-to-noise ratio for a given time is the mean brightness of the set of eight data points nearest to it divided by their standard deviation. Note that the signal-to-noise calculations at the approximate start and end of the transits are therefore inaccurate, because the calculations refer to the variation of data points on both sides of the transit simultaneously.

The figure below shows the signal-to-noise ratio for the observation of TrES-5-b, which required a minimum signal-to-noise ratio of 49 to detect. The dip in SNR at around 3:40 to 3:45 corresponds to the groups of data that intersect the possible observed end of the transit. The signal-to-noise ratio is better in the middle of the observation session, which corresponded to when the sky was clear rather than partially cloudy.
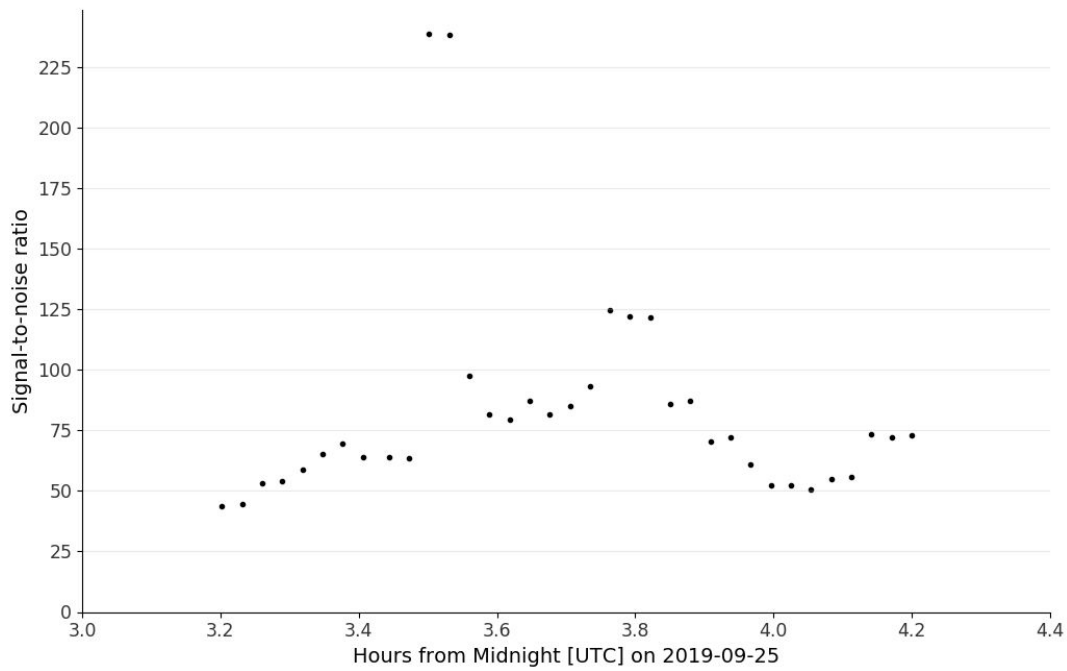
Fig.14: Estimated signal-to-noise ratio for the 2019-09-25 night of observation. The SNR is generally higher in the middle of the observation session.

The figure below shows the signal-to-noise ratio for the observation of HAT-P-23-b, which required a minimum signal-to-noise ratio of 71 to detect. Although the sky only became hazy at the end of the night, the signal-to-noise ratio varies by a factor of seven throughout the night. Considering that the predicted signal-to-noise ratio was 300, any ratio higher than 300 is likely due to chance alignment of the data, where the set of eight data points just happened to all agree precisely. This factor of seven variation in the signal-to-noise ratio is therefore also likely due to random alignment of the data.
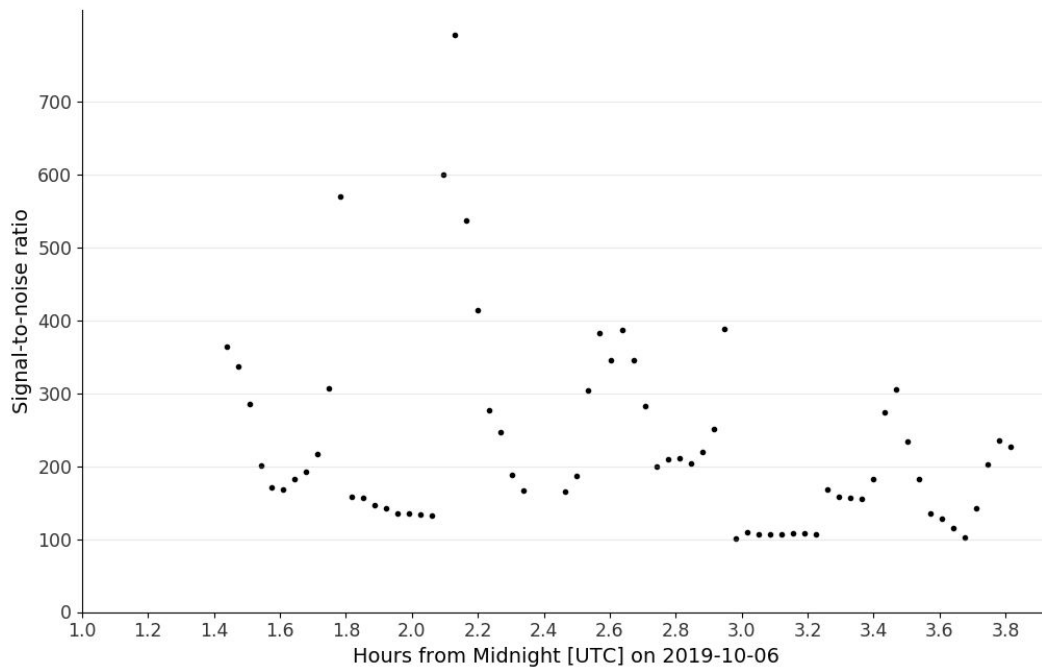
Fig.15: Estimated signal-to-noise ratio for the 2019-10-06 night of observation. SNR varies by a factor of seven throughout the night, despite that the sky is mostly clear throughout the night.

The next figure shows the signal-to-noise ratio for the observation of Kepler-412-b, which required a minimum signal-to-noise ratio of 96 to detect, but was not observed. The signal-to-noise ratio remained between 200 and 400 throughout the night, suggesting that the transit ought to have been observed.
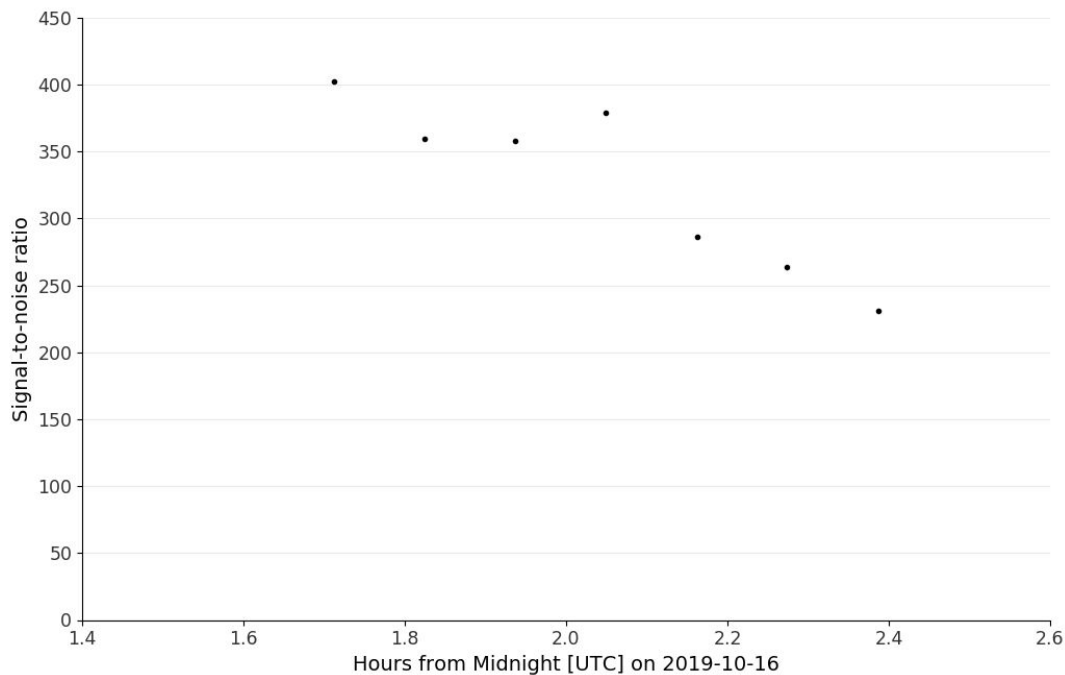
Fig.16: Estimated signal-to-noise ratio for the 2019-10-16 night of observation. The signal-to-noise ratio should have been sufficient to detect the transit.

The transit of Kepler-412-b was not detected, even though it should have been. The best explanation for this result is that the transit may have ended after the observations ended. This explanation would require that the transit end approximately 18 or minutes after the predicted time, which is plausible given the 9, 17, and 20 minute timing discrepancies observed in the transits of TrES-5-b and HAT-P-23-b. Timing errors are further discussed in Section 5.5.

4.4.3.   Transit and baseline brightness calculations

With these data, there are two methods of interest to calculate the baseline brightness and transit brightness of each exoplanet host star: weighted mean calculation, and unweighted mean calculation. The first method is to group the signal-to-noise ratio data bins from above into pre-transit and post-transit sections, and then to calculate a weighted transit mean and baseline mean using the mean of the individual data bins in each of those sections and the standard deviation of bins in each of those sections. The second method is to simply take the mean and standard deviation of the one bin during the transit that has the greatest signal-to-noise ratio and the one bin after the transit that has the greatest signal-to-noise ratio. Before transit and after transit sections are determined visually using the possible transit ingress and egress times from the light curves of Section 4.4.1.

The second method is more relevant for this analysis. The first method would be acceptable, except that for the low-SNR sections of the data, the data may not only have a high variance but also could also be offset from the true mean due to the same factors causing the lower signal-to-noise ratio. Due to this possibility, the following analysis instead uses the second method. The following analysis therefore calculates an unweighted transit mean and baseline mean from the portions of the data with the highest SNR.

The following table displays the mean and the standard deviation of the transit brightness and baseline brightness for each night of data, which are calculated from the highest-SNR data bins. Although it was concluded that the transit of Kepler-412-b was not observed, its values are included for completeness, assuming that the predicted transit end marked the actual transit end. Eight data points were chosen for the first night of data because the high-SNR portion of the data only spans approximately eight data points for each section of the transit. Eight data points were chosen for the second night of data because only approximately eight data points measure the transit baseline on either side of the transit. Three data points were chosen for the last night of data because only three data points fell after the predicted transit end.

Table 4: Transit and baseline brightnesses and standard deviations TrES-5-b and HAT-P-23b.

Exoplanet	Transit brightness	Transit std. dev.	Baseline brightness	Baseline std. dev.	Data points used for each
TrES-5-b	0.9836	0.006378	1.0051	0.005491	8
HAT-P-23-b	0.9964	0.001028	1.0125	0.003009	8
Kepler-412-b	1.0003	0.002646	1.0016	0.001543	3

4.4.4.   Transit light curves
The following figures contain the same data as the transit light curves of section 4.4.1., but overlaid are the transit and baseline brightnesses and standard deviations.
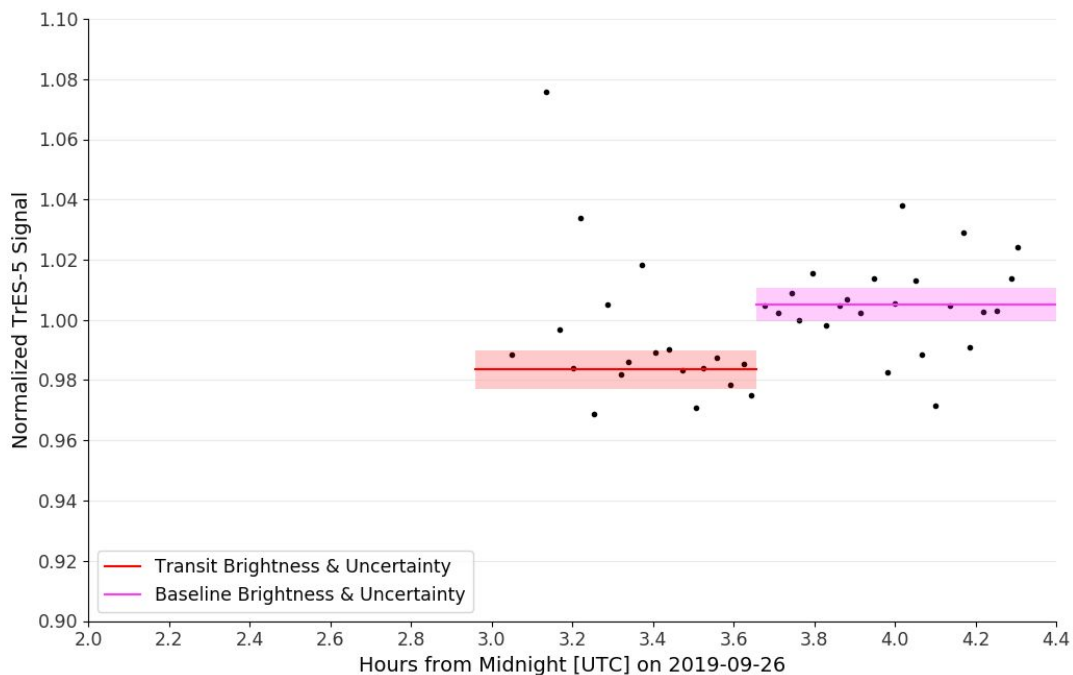
Fig.17: TrES-5-b transit with indicated mean brightness and uncertainty. Although the data are noisy, some semblance of a transit is noticeable.
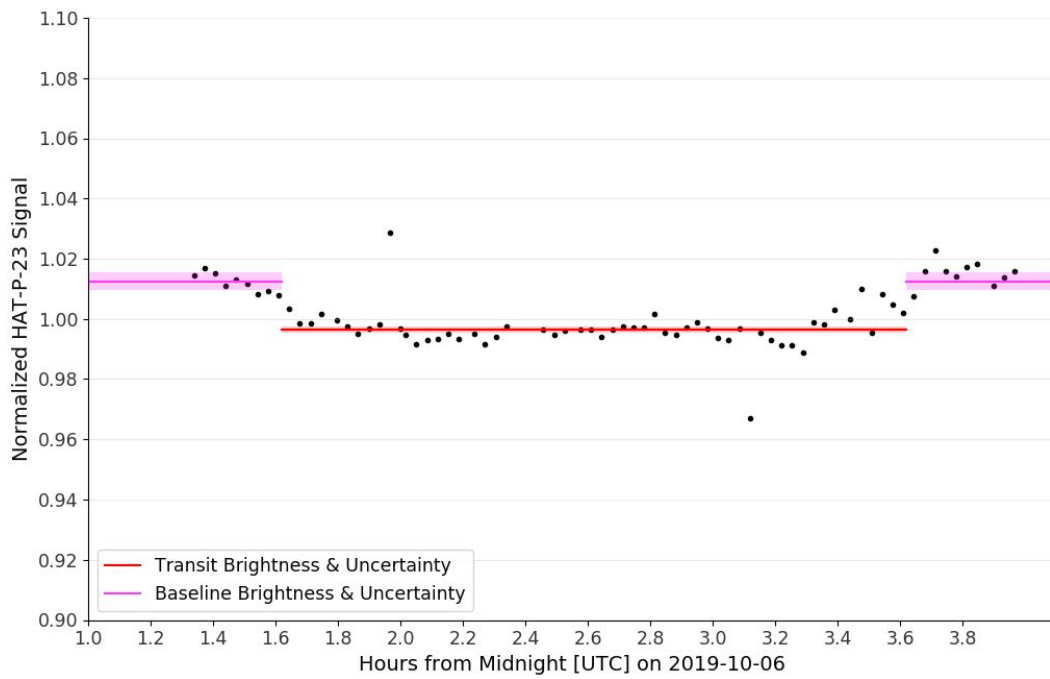
Fig.18: HAT-P-23-b transit with indicated mean brightness and uncertainty. It appears that a full transit is observable.
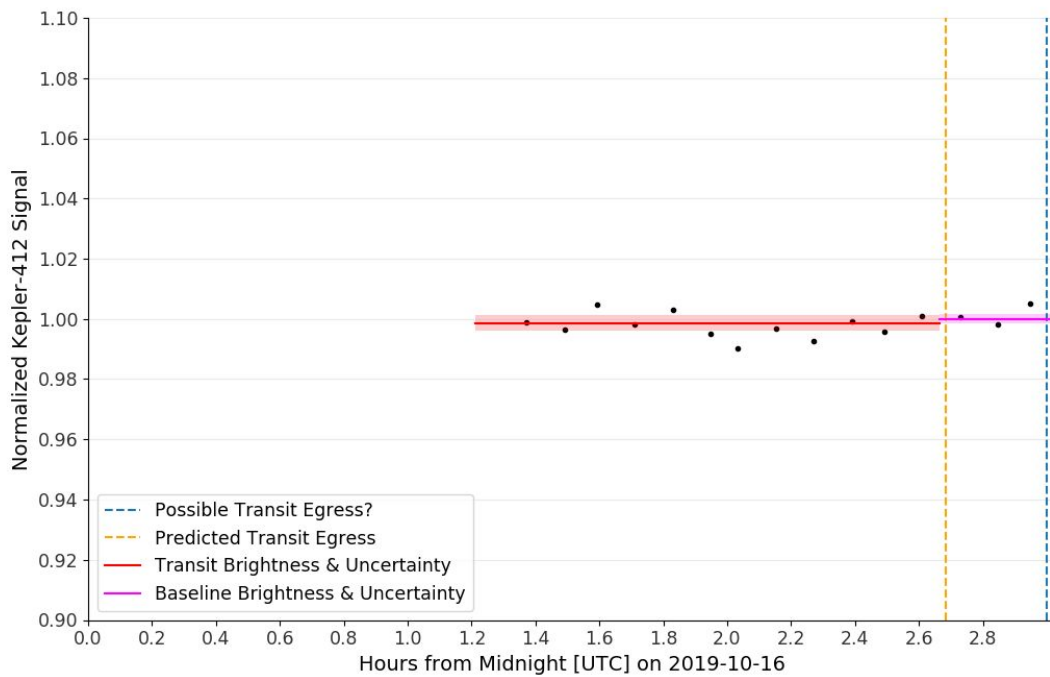

Fig.19: Kepler-412-b transit with indicated mean brightness and uncertainty using the predicted transit egress time. A proposed earliest actual transit egress time is shown in blue.

5. Analysis
5.1. Statistical significance of transits

The relevant statistical test to use to determine whether the baseline brightness was different from the transit brightness for each transit is the one-tailed two-sample student t-test. Fewer than 30 data points were used to estimate transit and baseline brightness for each exoplanet transit, and the sample means and variances are unequal. This reasoning is why the t-test is two-sampled rather than one-sampled. Since it is known that the brightness will decrease at the start of the transit and increase at the end of the transit, the test is one-tailed rather than two-tailed. The equations for calculating the test statistic and degrees of freedom for this significance test are as follows:

$$t = \frac{\overline{x_1} - \overline{x_2}}{\sqrt{\frac{s_1^2}{n_1} + \frac{s_2^2}{n_2}}} \text{ , and} \tag{7}$$

$$d.f. = \frac{(\frac{s_1^2}{n_1} + \frac{s_2^2}{n_2})^2}{\frac{(s_1^2/n_1)^2}{n_1 - 1} - \frac{(s_2^2/n_2)^2}{n_2 - 1}} \text{ ,} \tag{8}$$

where s is the sample standard deviation, n is the number of data points in each sample, and x is the average value (in this case, the average baseline brightness and average transit brightness). "1" denotes these values for the transit brightness; "2" denotes these values for the baseline brightness. The null hypothesis is that the two means, the transit brightness and baseline brightness, have no statistically significant difference.

The table below gives the test statistic, degrees of freedom, alpha, and resulting conclusion of the statistical test to determine the significance of each transit.

Table 5: Statistical significance of each transit

Exoplanet	t	d.f.	α	Confidence level	Statistically significant?
TrES-5-b	0.5596	14	0.29	71%	No
HAT-P-23-b	0.6793	14	0.26	74%	No
Kepler-412-b	0.0356	4	0.49	51%	No

5.2. Transit depths
Transit depths are calculated as follows:

$$transit\ depth\ (\%) = relative\ baseline\ brightness - transit\ baseline\ brightness \tag{9}$$

Error propagation suggests that transit depth standard deviations are as follows:

$$\sigma_{depth} = \sqrt{\sigma_{baseline}^2 + \sigma_{transit}^2} \text{ .} \tag{10}$$

Transit depths of each exoplanet, compared to their predicted depths, are displayed in the table below. Predicted transit depths in the table are from Jensen (2013).

Table 6: Transit depths and standard deviation

Exoplanet	Calculated transit depth (%)	Transit depth uncertainty (%)	Predicted transit depth (%)
TrES-5-b	2.16	0.84	2.04
HAT-P-23-b	1.53	0.32	1.40
Kepler-412-b	0.13	0.31	1.04

These data suggests the use of another statistical significance test to determine whether the transit depths differ from the predicted transit depths. The test to use here is a two-tailed one-sample student t-test, since the calculated transit depth represents a sample of data that physically could be greater or less than the predicted value. The null hypothesis is that the calculated transit depths do not differ from the predicted transit depths.

The equations for calculating the test statistic and degrees of freedom for this significance test are as follows:

$$t = \frac{|\bar{x} - \mu_0|}{s/\sqrt{n}} \ . \tag{11}$$

$$d.f. = n - 1 \ . \tag{12}$$

The table below describes the statistical significance of whether the observed transit depth differed from the predicted transit depth. Note that the transit depth test is only carried out for Kepler-412-b for the sake of completion, since it was determined that the transit ended after the observations ended. As a result, the transit depth of Kepler-412-b is the only one that is statistically different than its predicted value, with a confidence level of 96%.

Table 7: Statistical significance of each transit depth

Exoplanet	t	d.f.	α	Confidence level	Statistically significant?
TrES-5-b	0.404	7	0.70	30%	No
HAT-P-23-b	1.149	7	0.29	71%	No
Kepler-412-b	4.151	2	0.04	96%	Yes

5.3. Planet size calculation

The fraction an exoplanet dims its star's light is equivalent to the fraction of the star's area it blocks, i.e., its fractional cross-sectional area compared to the star. Since the planet and star radii are proportional to the square root of their area, planet sizes are calculated as follows (Perryman 2011):

$$\frac{Planet\ radius^2}{Star\ radius^2} = Transit\ depth \ . \tag{13}$$

$$Planet\ radius = Star\ radius * \sqrt{Transit\ depth} \ . \tag{14}$$

Measuring the luminosity and surface temperature of the star determines the star's radius (Perryman, 2011).

Here, error propagation suggests that planet radii uncertainties are as follows:

$$\sigma_{planet\ radius} = \sqrt{transit\ depth * \sigma_{star\ radius}^2 + \frac{star\ radius^2}{4*transit\ depth} * \sigma_{transit\ depth}^2}, \qquad (15)$$

Which is derived from the following general error propagation equation as applied to Eqn. (14):

$$\sigma_u = \sqrt{(\tfrac{\partial u}{\partial x})^2 \sigma_x + (\tfrac{\partial u}{\partial y})^2 \sigma_y}. \qquad (16)$$

The table below displays the planet sizes and their uncertainties from these calculations. Stellar radius and uncertainty for TrES-5 are from Maciejewski (2016). Stellar radius and uncertainty for HAT-P-23 and Kepler-412 are from Schneider (2019).

Table 8: Planet sizes and standard deviation

Exoplanet	Transit depth	Star radius (R_{sun})	Star radius standard deviation (R_{sun})	Planet radius (R_{Jup})	Planet radius standard deviation (R_{Jup})
TrES-5-b	0.0216	0.851	0.013	1.22	0.24
HAT-P-23-b	0.0153	1.20	0.07	1.44	0.17
Kepler-412-b	0.0013	1.29	0.04	0.45	0.54

Since planet radii are computed from transit depth and use the same star radius as studies in the literature, tests of statistical significance of the difference in calculated and predicted planet radii are interchangeable with the statistical tests for the difference in calculated and predicted transit depth. Therefore statistical tests of planet radii will therefore not be completed here.

5.4. Transit duration estimate
Since it is apparent that a full transit of exoplanet HAT-P-23-b was possibly observed, it is pertinent to calculate an estimate of the duration of the transit. Ingress and egress times and their uncertainties are ascertained by eye from the transit light curve. The ingress time was approximately 1.6±0.1 hours after midnight, and the egress time was approximately 3.6±0.2 hours after midnight. Therefore, the transit duration is 2.0±0.22 hours. The transit duration determined by Bakos (2014) was 2.179±0.017 hours. Since the calculated transit duration does not differ from that of the literature by more than one standard deviation, the two values are determined to be not statistically different.

5.5. Transit timing errors
In the observations, observed transit ingress and egress times consistently differed from predicted transit ingress and egress times by as much as 20 minutes. Specifically, for TrES-5-b, the observed egress time was 20 minutes early; for HAT-P-23-b, the observed ingress time was 17 minutes late and the observed egress time was 9 minutes late; for Kepler-412-b, the

estimated egress time was likely at least 18 minutes late. Timing uncertainty for the predicted transit ingress and egress is determined as per the following equations:

$$\# \ of \ periods = \frac{time \ passed \ since \ orbital \ period \ was \ determined}{orbital \ period} \text{, and} \qquad (17)$$

$$timing \ uncertainty = number \ of \ periods * \frac{orbital \ period \ uncertainty}{orbital \ period} \text{.} \qquad (18)$$

The timing uncertainty was determined to be 17 seconds for TrES-5-b (Maciejewski, 2016), 5.4 minutes for HAT-P-23-b (Bakos, 2014), and 4 seconds for Kepler-412-b (Deleuil, 2014). These timing uncertainties are small compared to the observed discrepancies between the predicted and observed times.

One possible explanation for the discrepancy in transit times is that the orbits of the planets could be eccentric, which would cause their transit timing to vary. This possibility is ruled out because the eccentricity of TrES-5-b is 0.017±0.012 (Maciejewski, 2016), and the eccentricity of Kepler-412-b is 0.004±0.003 (Deleuil, 2014), which both indicate nearly circular orbits. The eccentricity of HAT-P-23-b was not found in literature but is expected to be similar.

Another possible explanation is that the timing was mixed up due to the change in position of the Earth in its orbit. This effect could account for as much of 16 minutes of difference in the transit timing, since it takes light 16 minutes to travel 2 AU, the diameter of Earth's orbit. However, this still could not fully explain the timing differences, since observed differences were sometimes more than 16 minutes. Furthermore, for the observed transit time to lag the predicted transit time by 16 minutes due to this effect, the exoplanet could only have been observed by looking directly through the sun.

A final possible explanation is that other exoplanets could exist in these solar systems. These exoplanets may influence the period of the primary exoplanet's orbit due to their gravitational attraction. In fact, the existence of TrES-5-c is currently under speculation (Sokov, 2018). Although the HAT-P-23 and Kepler-412 systems do not yet appear to contain other exoplanets, such exoplanets may have periods on the order of dozens to hundreds of days, and would require focused long-duration studies to determine their existence.

6.   Conclusions
6.1.   Process
Results were obtained by performing image processing with acquired biases and darks and staff-provided flats, plate solving each light frame to obtain coordinates for each pixel, and performing virtual aperture photometry with on-chip reference stars. Transit brightnesses and baseline brightnesses were calculated from the set of data points representing those with the highest signal-to-noise ratio.

6.2.   TrES-5-b
The difference in transit brightness and baseline brightness of TrES-5 was only statistically significant at the 29% level. TrES-5-b's transit depth was determined to be 2.16±0.84%, which corresponds to a planetary radius of 1.22±0.24 R_{Jup}. The transit depth was found to be not statistically different from the transit depth in the literature of 2.04% (Jensen 2013). TrES-5-b's transit duration cannot be estimated from the data due to the observation of only a partial transit.

6.3.   HAT-P-23-b
The difference in transit brightness and baseline brightness of HAT-P-23 was only statistically significant at the 26% level. HAT-P-23-b's transit depth was determined to be 1.53±0.32%, which corresponds to a planetary radius of 1.44±0.17 R_{Jup}. The transit depth was found to be not statistically different from the transit depth in the literature of 1.40% (Jensen 2013). The transit duration of HAT-P-23-b was determined to be 2.0±0.22 hours, which was also found to be not statistically different from the transit duration in the literature of 2.179±0.017 hours (Bakos 2014).

6.4.   Kepler-412-b
The difference in transit brightness and baseline brightness of Kepler-412 was statistically insignificant, with a significance level of 49%. The transit depth was found to be statistically significant at a 4% level from the transit depth in the literature of 1.04%; however, the likeliest explanation for this result is that the transit egress occurred 18 minutes or more later than predicted, resulting in the observations missing the end of the transit. TrES-5-b's transit duration cannot be estimated from the data due to the observation of only a partial transit.

6.5.   Conclusory comments and recommendations for future observers
In this study, we observed the transits of TrES-5-b and HAT-P-23-b, two hot Jupiters each approximately 20% and 40% larger than Jupiter in radius respectively. In the process of collecting and analyzing data, we found that transit timing estimation is more unpredictable than expected. For best results, it is recommended to take at least a half an hour of observations before or after the transit. Skimping on these observations risks missing the start or end of the transit entirely.

7.   Acknowledgements

8. Appendices
8.1. Light frame reduction code

```
"""

Written by Alex Koenig

Instructions

1. In the code below, specify:
    File naming conventions
    Start & end file numbers for bias, dark, lights
    Flat file name
    Exposure time

2. Run this file

"""



from astropy.io import fits
import numpy as np
import os

Pre = "cal-"
Fix1 = ".000secsDarkOpen.00000"
Fix2 = ".000secsLightOpen.00000"
Prefix = "cal-0.000secsBiasOpen.00000"
Postfix = ".fit"
flatfile = 'p2-MasterFlat-Open.fit'

def make_master_bias(first_bias_file, last_bias_file):
    """

    Creates a list of bias files
    Takes their median

    Returns a Master Bias
    """
    bias_numbers = [first_bias_file+i for i in range(last_bias_file-first_bias_file+1)]
    bias_list = [str(Prefix+str(i)+Postfix) for i in bias_numbers]
    bias_stack = []
    for file in bias_list:
        bias_stack.append(fits.getdata(file))

    hdu = fits.PrimaryHDU(np.median(bias_stack, axis=0))
    hdu.writeto("MasterBias")

    return np.median(bias_stack, axis=0)

def make_master_dark(first_dark_file, last_dark_file, exposure_time_secs):
```

```python
    """
    Creates a list of dark files
    Takes their median & subtracts the Master Bias frame

    Returns a Master Dark
    """
    dark_numbers = [first_dark_file+i for i in range(last_dark_file-first_dark_file+1)]
    dark_list = [str(Pre+str(exposure_time_secs)+Fix1+str(i)+Postfix) for i in
dark_numbers]
    dark_stack = []
    for file in dark_list:
        dark_stack.append(fits.getdata(file))

    hdu = fits.PrimaryHDU(np.median(dark_stack, axis=0))
    hdu.writeto("MasterDark")

    return np.median(dark_stack, axis=0) - masterBias

def make_master_flat(flatfile):
    """
    Takes a master flat
    Divides each pixel by the mean of the central 100x100 pixels

    Returns a normalized master flat
    """
    #get the data from the flat file
    data,header = fits.getdata(flatfile,header=True)
    masterFlat = data

    #divide each pixel by the mean of the flat in the central 100 pixels
    x,y = int(len(masterFlat)/2), int(len(masterFlat[0])/2)
    centralMean = 0
    for i in range(100):
        for j in range(100):
            centralMean += masterFlat[x+i-50][y+i-50]
    centralMean/=100**2
    masterFlat = masterFlat/centralMean

    #Also save the edited flat file for the sake of (1) later re-use and (2) visual verification
of the flat
    hdu = fits.PrimaryHDU(masterFlat,header=header)
    hdu.writeto("MasterFlat")

    #return the masterFlat data
    return masterFlat

def make_light_list(first_light_file, last_light_file, exposure_time_secs):
    light_numbers = [first_light_file+i for i in range(last_light_file-first_light_file+1)]
```

```python
    light_list = [str(Pre+str(exposure_time_secs)+Fix2+str(i)+Postfix) for i in
light_numbers]
    return light_list

def apply_calibration_files(light_list, masterBias, masterDark, masterFlat):
    """
    Takes a master bias, dark, and flat, along with a list of light frames to calibrate
    Subtracts the master bias and master dark from each light frame, and then divides the
light frame by the master flat

    Creates a new calibrated file for each light frame
    """
    #for each of the light frames, perform the data calibration
    for file in light_list:
        data,header = fits.getdata(file,header=True)
        # subtract masterBias and masterDark, and then divide everything by the
masterFlat
        data = (data - masterBias - masterDark) / masterFlat
        hdu = fits.PrimaryHDU(data,header=header)
        hdu.writeto("calibrated_" + file)

if __name__ == "__main__":
    os.system("cp /home/alex/Documents/wao_data/raw_data/20190924p2/*
/home/alex/Documents/classes/8.287/py_code")
    os.system("cp /home/alex/Documents/wao_data/raw_data/p2-MasterFlat-Open.fit
/home/alex/Documents/classes/8.287/py_code")

    #Specify which bias, dark, and light files to use
    first_bias_file, last_bias_file = 508,527
    first_dark_file, last_dark_file = 759,762
    first_light_file, last_light_file = 700,741
    exposure_time = 100

    #Create the master bias frame
    masterBias = make_master_bias(first_bias_file, last_bias_file)

    #Create the master dark frame
    masterDark = make_master_dark(first_dark_file, last_dark_file, exposure_time)

    #Create the master flat frame
    masterFlat = make_master_flat(flatfile)

    #Create the list of light files to use
    light_list = make_light_list(first_light_file, last_light_file, exposure_time)

    #Calibrate each light file
    apply_calibration_files(light_list,masterBias,masterDark,masterFlat)
```

```
    os.system("rm cal-*")
    os.system("rm p2*")
    os.system("mv /home/alex/Documents/classes/8.287/py_code/calibrated*
/home/alex/Documents/wao_data/20190924p2/noise_calibrated_lights/")
    os.system("mv /home/alex/Documents/classes/8.287/py_code/Master*
/home/alex/Documents/wao_data/20190924p2/")
```

8.2.   Plate solving code

```
"""
```
Written by Alex Koenig

Instructions

1. Run command to install astrometry software, if not already installed
    sudo apt-get install astrometry.net

2. Download appropriate index files
    See http://astrometry.net/doc/readme.html
    Take two files, each ~1/5th of field size, at appropriate sky location
    Eg 2.8-4.0 arcmin and 4.0-5.6 arcmin for a field size of 20 arcmin

3. Move index files into astrometry folder
    Probably installed at /usr/local/astrometry/data/

4. Create a parameters file
    create backend.cfg in /usr/local/astrometry/data/

    In the index file, write:
        add_path /usr/local/astrometry/data
        index index-4201-13.fits
        index index-4202-13.fits

    (fill in actual index files used)

5. Specify parameters in the code below
    RA,Dec of the approximate center of the image
    Search Radius
    Origin and output directories
    File names

6. Run this file

```
"""
```

```
import os
```

```
#RA,Dec of the center of the image
RA = 305.2205 #deg
```

```
Dec = 59.4487 #deg

#Plate solver assumes image degree width between 0.2 and 0.5

#Specify a radius to search in degrees
SearchRadius = 0.5

#File naming and location
Prefix = "calibrated_cal-100.000secsLightOpen.00000"
Postfix = ".fit"
OriginFolder = "/home/alex/Documents/wao_data/20190924p2/noise_calibrated_lights/"
OutputFolder =
"/home/alex/Documents/wao_data/20190924p2/astrometry_calibration_files/"
OutputFolder_endFiles =
"/home/alex/Documents/wao_data/20190924p2/astrometry_calibrated_lights"

#File numbering
StartingFileNumber = 700    #INPUT BY USER
EndFileNumber = 741         #INPUT BY USER
NumFiles = EndFileNumber - StartingFileNumber + 1

#Create a list of file names to perform astrometry on
NumberList = range(NumFiles)
FileNumberList = []
for i in range(NumFiles):
    FileNumberList.append(StartingFileNumber+NumberList[i])
FileNameList = []
for i in range(NumFiles):
    FileNameList.append(Prefix+str(FileNumberList[i]))

#perform astrometry on each image
for image in FileNameList:
    os.system("solve-field --dir "+OutputFolder+" --scale-units degwidth --scale-low 0.2
--scale-high 0.5 --ra "+str(RA)+", --dec "+str(Dec)+", --radius "+str(SearchRadius)+"
--overwrite --backend-config /usr/local/astrometry/etc/backend.cfg
"+OriginFolder+image+Postfix)
    #move the relevant files to the end folder & rename
    os.system("mv "+OutputFolder+image+".new "+OutputFolder_endFiles)
    os.system("cd "+OutputFolder_endFiles+" && rename 's/"+Prefix+"//' *.new")
```

8.3.   Photometric analysis code
```
"""
```
Written by Alex Koenig

Instructions

1. In the code below, specify:
    File numbers

Coordinates of host star and reference stars
        Which function to run

2. Run this file

"""

```python
from astropy.io import fits
from astropy import wcs
from photutils import CircularAperture, CircularAnnulus, aperture_photometry
import matplotlib.pyplot as plt
import numpy as np

def ReadData(ShowImage = False):
    start_file_num = 700
    end_file_num = 741

    num_files = end_file_num-start_file_num+1

    RA_star = 305.221829
    Dec_star = 59.44923

    RA_ref1 = 305.2659
    Dec_ref1 = 59.52752

    RA_ref2 = 305.44515
    Dec_ref2 = 59.42362

    RA_ref3 = 305.285163
    Dec_ref3 = 59.428284

    RA_ref4 = 305.39247
    Dec_ref4 = 59.43846

    RA_ref5 = 305.03526
    Dec_ref5 = 59.447903

    RA_ref6 = 305.277008
    Dec_ref6 = 59.3401803

    coords = [(RA_star,Dec_star),(RA_ref1,Dec_ref1),(RA_ref2,Dec_ref2),(RA_ref3,Dec_ref3),(RA_ref4,Dec_ref4),(RA_ref5,Dec_ref5),(RA_ref6,Dec_ref6)]

    R1,R2,R3 = 7.8,10,12

    star = []
    RefStar1 = []
```

```python
RefStar2 = []
RefStar3 = []
RefStar4 = []
RefStar5 = []
RefStar6 = []
file_list = []
time_list = []

for data_num in range(num_files):
    #read file
    file_list.append(data_num+start_file_num)
    num_str = str(data_num+start_file_num)
    data_str = num_str+'.new'

    w = wcs.WCS(data_str)
    coordinates = []
    for i in range(7):
        coordinates.append((w.all_world2pix(coords[i][0],coords[i][1],0)))

    #R1,R2,R3 = 5,9,12
    apertures = CircularAperture(coordinates,r=R1)
    annulus_apertures = CircularAnnulus(coordinates, r_in=R2, r_out=R3)
    apers = [apertures, annulus_apertures]

    data,header = fits.getdata(data_str, header=True)
    time_list.append(header["DATE-OBS"])
    phot_table = aperture_photometry(data,apers)

    bkg_mean = phot_table['aperture_sum_1'] / annulus_apertures.area
    bkg_sum = bkg_mean * apertures.area
    final_sum = phot_table['aperture_sum_0'] - bkg_sum
    phot_table['residual_aperture_sum'] = final_sum

    star.append(final_sum[0])
    RefStar1.append(final_sum[1])
    RefStar2.append(final_sum[2])
    RefStar3.append(final_sum[3])
    RefStar4.append(final_sum[4])
    RefStar5.append(final_sum[5])
    RefStar6.append(final_sum[6])

    if(ShowImage):
        if data_num == 0:
            ax = plt.gca()
            c0 = plt.Circle(coordinates[0], R1, color='black', fill=False)
            c1 = plt.Circle(coordinates[1], R1, color='r', fill=False)
            c2 = plt.Circle(coordinates[2], R1, color='g', fill=False)
            c3 = plt.Circle(coordinates[3], R1, color='b', fill=False)
```

```python
        c4 = plt.Circle(coordinates[4], R1, color='orange', fill=False)
        ax.add_artist(c0)
        ax.add_artist(c1)
        ax.add_artist(c2)
        ax.add_artist(c3)
        ax.add_artist(c4)
        plt.imshow(data,cmap='binary')
        plt.show()


    return file_list, time_list,
[np.asarray(star),np.asarray(RefStar1),np.asarray(RefStar2),np.asarray(RefStar3),np.as
array(RefStar4),np.asarray(RefStar5),np.asarray(RefStar6)]


def CreateLightCurve(References, TimeList, time_conversion = False):
    WeightedReference = StarList[0] - StarList[0]
    for i in range(len(StarList)):
        if i in References:
            WeightedReference += StarList[i]/np.mean(StarList[i])
    Signal = StarList[0] / np.mean(StarList[0])*(len(References)) / WeightedReference

    plt.figure(figsize=(12,7.5),dpi=100)
    plt.style.use('default')
    plt.rc('font',family='sans-serif')
    if time_conversion:
        plt.scatter(TimeList,Signal, c='black',marker='.')
    else:
        plt.scatter(range(len(Signal)), Signal, c='black',marker='.')
    plt.xlabel('Hours from Midnight [UTC] on 2019-09-26',fontsize=14)
    #plt.xlim(0,16)
    plt.ylabel('Normalized TrES-5 Signal',fontsize=14)
    #plt.title('Exoplanet transit light curve',fontsize=22)
    plt.grid(axis='y',alpha=.25)
    plt.xticks(fontsize=12.5,alpha=0.8)
    plt.xticks(np.arange(2, 4.5, 0.2))
    plt.yticks(fontsize=12.5,alpha=0.8)
    plt.yticks(np.arange(0.9, 1.1, 0.02))
    plt.ylim(0.9,1.1)
    plt.gca().spines['top'].set_alpha(0)
    plt.gca().spines['right'].set_alpha(0)

    #plt.axvline(x=2.2, linestyle = '--', label='Predicted Transit Ingress & Egress',
color='orange')
    #plt.axvline(x=4.0, linestyle = '--',color='orange')
    #plt.axvline(x=3.66, linestyle = '--', label='Possible Observed Transit Egress')

    plt.axhline(y=0.9836, xmin = 0.4, xmax = 0.69, label = 'Transit Brightness &
Uncertainty', c='red')
```

```python
    plt.axhline(y=1.0051, xmin=0.69, xmax=1, label = 'Baseline Brightness & Uncertainty',
c='magenta')
    plt.axhspan(ymin=.9836-.0064, ymax=.9836+.0064, xmin=0.4,xmax=0.69, alpha=0.2,
facecolor='red')
    plt.axhspan(ymin=1.0051-.0055, ymax=1.0051+.0055, xmin=.69, xmax=1, alpha=0.2,
facecolor='magenta')
    #plt.axvspan(xmin=2, xmax=3.66, ymin = (0.9836-1)*5 + 0.5, ymax =
(1.0051-1)*5+0.5, label = 'Transit Depth', alpha=0.2, facecolor='orange')

    plt.legend(fontsize=12.5, loc=3)
    plt.show()

    for sig in Signal:
        print(sig)

def PlotRelativeSignal(star1, star2):
    mean = np.mean(StarList[star1] / StarList[star2])
    RelativeSignal = StarList[star1] / StarList[star2] / mean
    plt.scatter(FileList,RelativeSignal)
    plt.xlabel('file num')
    plt.ylabel('relative photon count')
    plt.ylim(0.8,1.2)
    plt.title('relative signal received between two stars in the frame')
    plt.show()

def VerifyReferenceStar(star):
    WeightedReference = StarList[0] - StarList[0]
    for i in range(len(StarList)-1):
        if i+1 != star:
            WeightedReference += StarList[i+1]/np.mean(StarList[i+1])
    Signal = StarList[star] / np.mean(StarList[star])*(len(StarList)-2) / WeightedReference
    plt.figure(figsize=(12,7.5),dpi=100)
    plt.scatter(range(len(FileList)),Signal, c='black', marker='.')
    plt.xlabel('Exposure number', fontsize = 14)
    plt.ylabel('Relative photon count between reference stars', fontsize = 14)
    plt.grid(axis='y',alpha=.25)
    plt.xticks(fontsize=12.5,alpha=0.8)
    plt.yticks(fontsize=12.5,alpha=0.8)
    plt.yticks(np.arange(0.9, 1.1, 0.02))
    plt.ylim(0.9,1.1)
    #plt.title('Reference star verification: stars should be constant')
    plt.show()


def PlotAllStars(Stars):
    for star in Stars:
        if star==4:
            plt.scatter(FileList,StarList[4], c='orange')
```

```python
            if star==3:
                plt.scatter(FileList,StarList[3], c='blue')
            if star==2:
                plt.scatter(FileList,StarList[2], c='green')
            if star==1:
                plt.scatter(FileList,StarList[1], c='red')
            if star==0:
                plt.scatter(FileList,StarList[0], c='black')
        plt.show()


if __name__ == '__main__':
    FileList,TimeList, StarList = ReadData(False)
    Time = []
    for time in TimeList:
        hour = float(int(time[11])*10+int(time[12]))
        minute = float(int(time[14])*10+int(time[15]))
        second = float(int(time[14])*10+int(time[15]))
        Time.append(hour + minute/60 + second/3600)
    print(Time)
    CreateLightCurve([1,2,3,4,5,6], Time, time_conversion=True)
    #PlotRelativeSignal(0,4)
    #PlotRelativeSignal(0,1)
    #PlotRelativeSignal(0,4)
    #VerifyReferenceStar(6)
    #PlotAllStars([0,1,2,3,4])
```
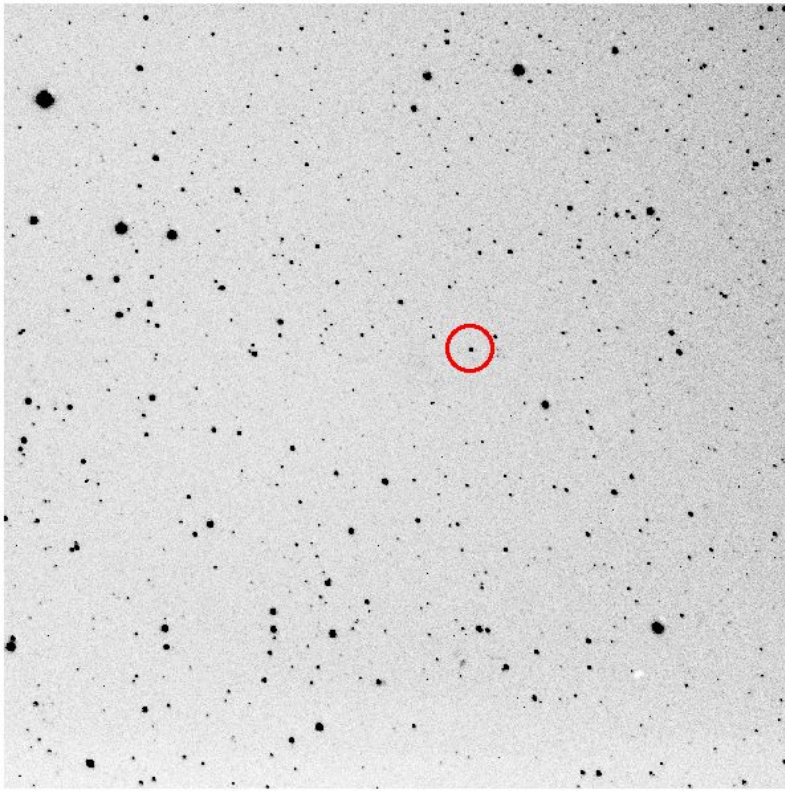
8.4. Sample light frames

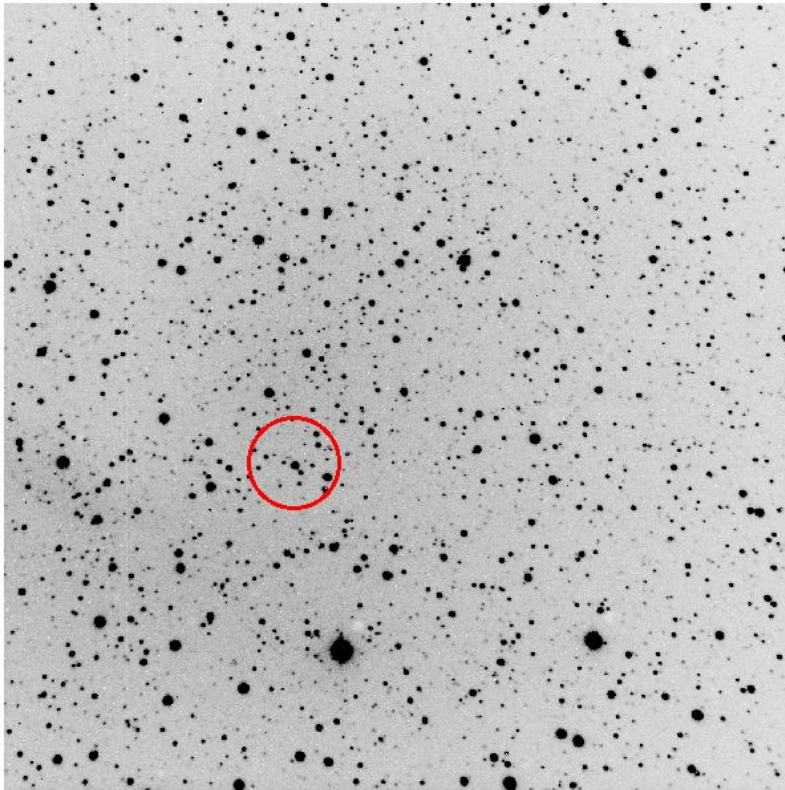Fig.20: Light frame of TrES-5. Inverted. Host star circled in red.

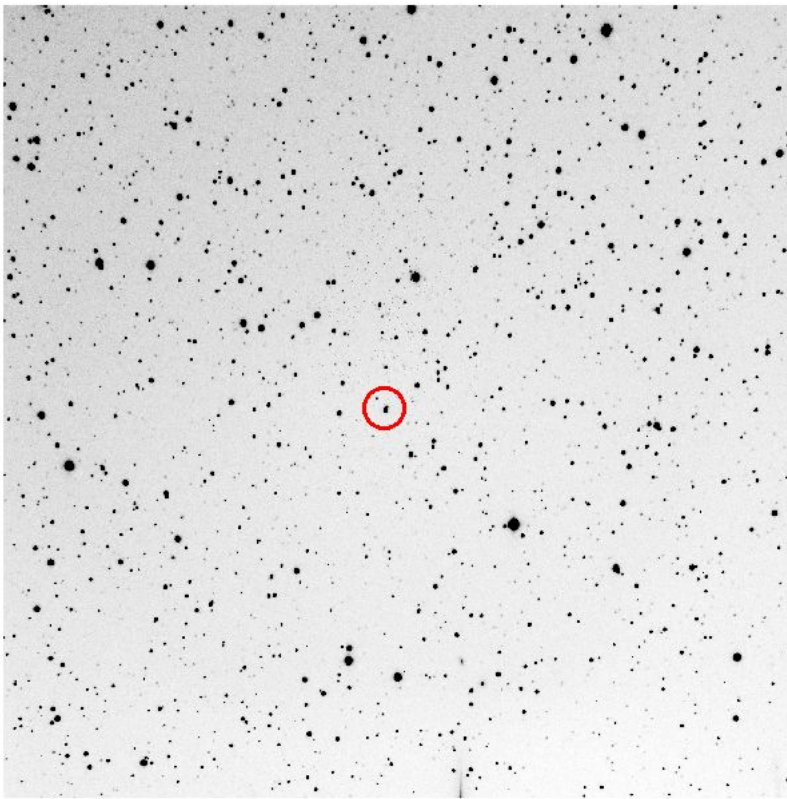Fig.21: Light frame of HAT-P-23. Inverted. Host star circled in red.

Fig.22: Light frame of Kepler-412. Inverted. Host star circled in red.

9. References

Angerhausen, D., et al. "A Comprehensive Study of Kepler Phase Curves and Secondary Eclipses: Temperatures and Albedos of Confirmed Kepler Giant Planets." Publications of the Astronomical Society of the Pacific, vol. 127, no. 957, 2015, pp. 1113–1130., doi:10.1086/683797.

Bakos, G.Á., et al., 2011. HAT-P-20b–HAT-P-23b: FOUR MASSIVE TRANSITING EXTRASOLAR PLANETS. The Astrophysical Journal 742, 116. doi:10.1088/0004-637x/742/2/116

Ciceri, S., et al., 2015. Physical properties of the HAT-P-23 and WASP-48 planetary systems from multi-colour photometry. Astronomy & Astrophysics 577. doi:10.1051/0004-6361/201425449

Cowley, M., 2014. Characterization of exoplanets by way of differential photometry.

Dawson, Rebekah I.; et al., 2018. "Origins of Hot Jupiters". Annual Review of Astronomy and Astrophysics. 56: 175–221. arXiv:1801.06117. doi:10.1146/annurev-astro-081817-051853.

Deleuil, M., et al. "SOPHIE Velocimetry Of Kepler transit Candidates XI. Kepler-412 System: Probing the Properties of a New Inflated Hot Jupiter." Astronomy & Astrophysics, vol. 564, Apr. 2014, doi:10.1051/0004-6361/201323017.

Fortney, J.J., et al., 2008. A Unified Theory for the Atmospheres of the Hot and Very Hot Jupiters: Two Classes of Irradiated Atmospheres. The Astrophysical Journal 678, 1419–1435. doi:10.1086/528370

Lang, D., et al., 2010. Astrometry.net: Blind astrometric calibration of arbitrary astronomical images. Astron. J. 139, 1782–1800. doi:10.1088/0004-6256/139/5/1782

Jensen, E., Exoplanet Transit Finder. Retrieved from https://astro.swarthmore.edu/transits.cgi on 2019-11-15.

Maciejewski, G., et al., 2016. "New transit observations for HAT-P-30 b, HAT-P-37 b, TrES-5 b, WASP-28 b, WASP-36 b, and WASP-39 b." Astronomy & Astrophysics.

Mislis, D., et al., 2015. "High-precision multiband time series photometry of exoplanets Qatar-1b and TrES-5b." Acta Astronomica, vol 66, no 1, p. 55-74.

Perryman, M. 2011, The Exoplanet Handbook, Cambridge University Press, New York; ISBN: 0521765595

Poddany, S., et al., 2010. New Astronomy 15, pp. 297-301, Exoplanet Transit Database. Reduction and processing of the photometric data of exoplanet transits

Schneider, J. "Interactive Extra-solar Planets Catalog". The Extrasolar Planets Encyclopedia. Retrieved 1 November 2019.

Sokov, E., et al. "Transit Timing Analysis of the Exoplanet TrES-5 b. Possible Existence of the Exoplanet TrES-5 c." Monthly Notices of the Royal Astronomical Society, vol. 480, no. 1, 2018, pp. 291–301., doi:10.1093/mnras/sty1615.

Wolszczan, A.; Frail, D. A. (1992). "A planetary system around the millisecond pulsar PSR1257 + 12". Nature. 355 (6356): 145–147. Bibcode:1992Natur.355..145W. doi:10.1038/355145a0.